Accepted Manuscript

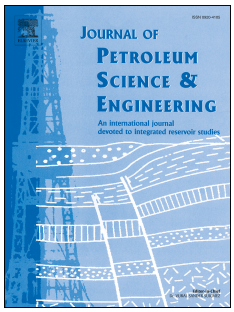

Diagenesis and reservoir quality of carbonates rocks and mixed siliciclastic as response of the Late Carboniferous glacio-eustatic fluctuation: A case study of Xiaohaizi Formation in western Tarim Basin

Mei-Yan Fu, Rong-Cai Song, Gluyas Jon, Shao-Nan Zhang, Qian Huang

PII: S0920-4105(19)30250-5

DOI: https://doi.org/10.1016/j.petrol.2019.03.011

Reference: PETROL 5861

To appear in: *Journal of Petroleum Science and Engineering*

Received Date: 5 June 2018

Revised Date: 13 February 2019

Accepted Date: 4 March 2019

Please cite this article as: Fu, M.-Y., Song, R.-C., Jon, G., Zhang, S.-N., Huang, Q., Diagenesis and reservoir quality of carbonates rocks and mixed siliciclastic as response of the Late Carboniferous glacio-eustatic fluctuation: A case study of Xiaohaizi Formation in western Tarim Basin, *Journal of Petroleum Science and Engineering* (2019), doi: https://doi.org/10.1016/j.petrol.2019.03.011.

Diagenesis and Reservoir Quality of Carbonates Rocks and Mixed siliciclastic as Response of the Late Carboniferous Glacio-Eustatic Fluctuation: A case study of Xiaohaizi Formation in Western Tarim Basin

FU MEI-YAN[1], SONG RONG-CAI[1*], JON GLUYAS[2], ZHANG SHAO-NAN[3], AND HUANG QIAN[1]

[1] *College of Energy Resources, Chengdu University of Technology, Chengdu 610059, China;*

[2.] *Department of Earth Science, Durham University, Durham, DH1 3LE, UK;*

[3] *College of Geosciences and Technology of Southwest Petroleum University, Chengdu 610500, China*

* Corresponding author: 417102145@qq.com

ABSTRACT: Late Carboniferous-Permian was a longest-lived and most widespread ice age. The depositional environment, diagenesis and reservoir quality of carbonate rocks as response to the glacio-eustatic changes was analyzed in this study. The Upper Carboniferous Xiaohaizi Formation in the western Tarim Basin is an important oil reservoir. The dolostones from the Xiaohaizi Formation have very good physical properties, with maximum porosity and permeability of 16.6% and 214mD, respectively. The sedimentary facies of the Xiaohaizi Formation consist of carbonate shoals and lagoon on a mixed siliciclastic-carbonate platform. There was a strong heterogeneity of carbonate rocks deposited on shoals. Porous dolostones always alternate with tight sparry allochemical limestones. Based on the petrographic observation and stable isotope measurement, the controlling factors for the heterogeneity and reservoir quality were revealed. The palaeosol, vadose silt, karst breccia, detrital

kaolinite, darkening of dolostones and enrichment of ^{18}O indicate the short-lasting subaerial emergence during the glacial period. During the glacial sea level fall, the mixed siliciclastic and carbonate allochems deposited on bioclastic and intraclastic shoals, while dolomitization of calcic grains occurred under a relatively low-temperature. Through the correlation analysis of physical property, lithology, rock components, it's suggested that the reservoir quality of the Xiaohaizi Formation was controlled by mixed sedimentation and dolomitization associated with glacio-eustatic fluctuation. At the burial diagenesis, the effect of hydrothermal fluid on physical properties of dolostones with relative high primary porosity was positive, whereas resulted in the poikilotopic calcite cementation. The assembly of fluorite, dickite and authigenic pyrite were indicators for hydrothermal fluid accumulation. The control of glacio-eustatic fluctuations on sedimentation and diagenesis in carbonates could be used to forecast the reservoir quality.

Keywords: **Carbonates; Mixed siliciclastic; Diagenesis; Reservoir Quality; Hydrothermal; Glacio-Eustatic**

INTRODUCTION

The glaciation successions on Gondwana supercontinent occurred at Carboniferous to Early Permian, resulting in glacio-eustatic sea level changes (Crowley and Baum 1991; Maynard and Leeder 1992; Butts 2005; Rygel et al. 2008; López-Gamundí and Buatois 2010). Assuming a constant rate of subsidence, glacio-eustatic sea level changes are recorded in the stacking patterns of facies and

lithologies, e.g. the assembly of subtidal carbonate, mixed carbonate and siliciclastic, and quartz arenite (Butts 2005), as well as the subaerial exposure and meteoric diagenesis (Bishop et al. 2009; Elrick and Scott 2010), through waxing and waning of glaciation. A similar stratigraphy sequence of the Upper Carboniferous was found in the western Tarim Basin, northwestern China (Jiang and Gu 2002; Fu et al. 2012a). The main lithologies of gas zone from the Late Carboniferous in the western Tarim Basin are limestones and dolostones deposited on a carbonate platform (Zhang et al. 2009; Ma et al. 2015).

Based on the carbonate sequence associated with the sea-level fluctuation, the early diagenetic fabric and reservoir quality could have been influenced by the relative sea-level change (Sun and Esteban 1994; McKay et al. 1995; Strasser and Strohmenger 1997; Taghavi et al. 2006; Morad et al. 2012). The geochemical conditions of early diagenesis generally depend on the duration of relative sea-level changes (Morad et al. 2012). The subaerial exposure and meteoric diagenesis of carbonate rocks during glacio-eustasy in the mid-Late Carboniferous is an important diagenetic process that contributes to improve reservoir quality by enhancing both the porosity and permeability (Butts 2005; Bishop et al. 2009; Elrick and Scott 2010; Ueno et al. 2013). On the onset of glacio-eustasy, carbonate rocks experience subaerial emergence and chemical weathering in the ephemeral freshwater lenses, resulting in the formation of vugs, dissolve pores and calcite cementation (Strasser and Strohmenger 1997; Wang and Al-Aasm 2002; Hiatt and Pufahl 2014; Ren and Jones 2016). However, with the relative sea-level rise, dolomitization was prone to

68 occur during transgressive system tract and early highstand system tract (Kordi et al.
69 2017). It has been suggested the dolomitization can be driven by sea water or
70 modified sea water (Qing et al. 2001; Machel 2004). The pervasive dolomitization can
71 be driven by periodically increased salinity response to relative sea-level fluctuation,
72 assuming in a semiarid or arid environment (Sun and Esteban 1994). However, the
73 diagenetic alteration and reservoir quality of carbonate rocks in response to the
74 glacio-eustatic fluctuation in the Late Carboniferous in Tarim plate are poorly
75 understood.

76 The impure carbonate rocks, containing a small amount of terrigenous detrital
77 grains, occurred in the Upper Carboniferous Xiaohaizi Formation, the western Tarim
78 Basin. The Carboniferous mixed sequence of dolostones, limestones, mudstones and
79 sandstones resulted from the glacio-eustatic fluctuation in the study area (Fig.1)(Fu et
80 al. 2012a). Based on the petrology and physical property, the mixed sedimentation
81 and diagenesis related to the glacio-eustatic fluctuation were discussed, and then
82 controlling factors for reservoir quality of these impure carbonate rocks were
83 analyzed.

84 ## GEOLOGICAL SETTING

85 Tarim Basin is a typical superimposed basin in the Western China (Fig.1a) (Li
86 et al. 1996). At the period of Carboniferous, the Tarim Plate drifted northward to a
87 latitude of twenty degrees north (Jia 2013). Transgression after Ordovician began to
88 inundate into the western Tarim Basin from west to east in the Early Carboniferous
89 (Fu et al. 2012a). The multiple phases of eustatic fluctuation as the consequence of

Gondwanan glaciation (Rygel et al. 2008; López-Gamundí and Buatois 2010) during Carboniferous resulted in the formation of mixed siliciclastic and carbonate sequence in the western Tarim Basin (Fig.1) (Xiao and Pan 1999). At the Late Carboniferous, transgression reached to the zenith. Consequently, limestones deposited on the carbonate platform across the whole basin (Zhu et al. 2002; Jiang and Yu 2003; Ma et al. 2015).

During the Late Carboniferous to the Early Permian, the Tarim Plate appears to have collided with Siberia and Kazakhstan (Scotese and McKerrow 1990). Consequently, an extensive basalt eruption occurred during the Permian period (Ernst and Buchan 2001; Li et al. 2011). Meanwhile, the extensional tectonic movement significantly influenced the Tarim Basin, resulting in the oil and gas migration and hydrothermal fluid accumulation (Zhang et al. 2011a).

Bachu-Makit area is located in the western Tarim Basin, including Bachu uplift and Makit slope (Fig.1A). Makit slope is dipping southwest. Bachu uplift belongs to the western part of the central paleo-uplift (Song et al. 2018). Bachu-Makit area is closed to the Awati Depression, where is one of the hydrocarbon generation centers in the Tarim Basin (Zhang et al. 2011a). Several oil and gas fields have been discovered in the Carboniferous reservoirs in the Bachu-Makit area, such as Yasongdi Field, Bashituo Field, Niaoshan Field, and so on (Tan et al. 2004; Zhang et al. 2011b; Zhu et al. 2013; Song et al. 2018). Bachu-Makit area is one of the volcano activity centers in the Tarim Basin at the Early Permian (Meng et al. 2011). There are two deep fractures

111 impenetrating from Cambrian to Permian (Li et al. 2015), e.g. Xianbazha fault and
112 Selibuya fault (Fig.1B).

113 The Carboniferous lithologic units in the Bachu-Makit area include the Bachu,
114 the Kalashayi and the Xiaohaizi formations (Fig.1C) from bottom to top. The
115 Xiaohaizi Formation is an important oil bearing zone in the study area. The burial
116 depth of the Xiaohaizi Formation ranges from 1944m to 4457m, with deeper depth
117 from east to west. As the consequence of mixed sedimentation, quartz and clay
118 mineral contents within carbonate rocks in the Xiaohaizi Formation are relatively high
119 (Zhu et al. 2002; Fu and Zhang 2011).

120 ## MATERIAL AND METHODS

121 In this study, the cores of six wells were collected from Petroleum Exploration
122 and Production Research Institute, Northwest Company, Sinopec Group, China. The
123 core description was carried on more than 130 meters drilling cores from six wells
124 (Table 1). The sedimentary structure, texture, color, and oil-bearing property were
125 described on these cores. Based on the cores description, the macro-scale cycle of
126 lithofacies was established (Fig.2).

127 179 thin sections were used for identification of mineralogy, diagenetic textures,
128 and diagenesis. Thin sections were examined for mineralogy using Alizarin Red and
129 potassium ferricyanide staining. Combining with the core description, the vertical
130 changes of lithology on the stratigraphic column of the Xiaohaizi Formation were
131 analyzed.

32 thin sections were observed under Cathode luminescence (CL), using CITL/CL8200 MK5-2 (made in England) cold cathode instrument. The voltage was 14 kV, and electric current is 380 μA. The CL images were captured with 20-second exposure times.

Scanning electron microscopy (SEM) petrography was performed using a Quanta 250 FEG (FEI Company, Hillsboro, OR, USA) with Oxford INCAx-max20 (Energy Disperse Spectroscopy, Oxford Instruments, Abingdon, England). These samples were coated with carbon, using secondary electron imaging. The resolution for secondary electron imaging under high vacuum is 2 nm, and that of backscattered electron imaging is 2.5 nm. The operating conditions were an accelerating voltage of 20kV, a filament current of 240μA, and beam diameter of 4 μm, and working distances of 10-20 mm.

A THMS 600 Cooling-Heating Stage (Linkam Scientific, Surrey, England) was used to measure the homogenization temperature (T_H) of fluid inclusion enclosed in the calcite cements. The temperature range of the instrument is from −196° to 600° C with a precision of <0.1 °C. The rate of temperature increase can be controlled to within 1 °C/min when approaching the critical point.

The composition of minerals was determined by using a Rigaku DMAX-3C x-ray diffractometer (Rigaku Corporation, Tokyo, Japan) equipped with Cu Kα radiation (40 kV, 20 mA). Angle accuracy is greater than 0.02° (2θ). The scanning speed was 0.05 s/step, and the scanning range was 3–50° (2θ). Semi-quantitative phase analysis

153 was performed by a PDF2 (2004) computer using Jada 5.0 software. The relative
154 deviation is less than 10% when the content of the mineral is more than 40%.
155 The composition of elements in carbonate rocks was detected by Optima 5300 V
156 Inductively Coupled Plasma atomic emission spectroscopy (ICP-AES) (Perkin-Elmer
157 Company) and Inductively Coupled Plasma mass spectrometry (ICP-MS). Aliquots of
158 100 mg of 13 bulk sample powders were dried at 100°C for two hours and dissolved
159 in mixed solutions composed of 4 mL hydrofluoric acid, 2mL hydrochloric acid, 3mL
160 nitric acid, 1mL perchloric acid and three drops of sulfuric acid. Then the samples
161 dissolved in solutions were heated to about 200 °C for four hour until the white smoke
162 occurring. The 5mL chloroazotic acids were added into the solutions to extract
163 elements. The solutions were transferred to a 50mL volumetric flask, diluting with
164 deionized water to volume. After that, the major elements were tested by ICP-AES
165 and minor elements were tested by ICP-MS.
166 A total of 10 carbonate rocks from well M10 were measured for their bulk
167 carbonate carbon and oxygen stable isotope values, measured by a MAT253 stable
168 isotope ratio mass spectrometer (Thermo Scientific, Waltham, MA, USA). All the
169 isotope data are reported as per-mil deviation from the Pee Dee Belemnite (PDB)
170 standard. Samples were processed with phosphoric acid method. The measuring
171 accuracy for ^{13}C is 0.0037‰, and that for ^{18}O is 0.013‰.
172 The gas method of Jannot and Lasseux (2012) was used to perform porosity and
173 permeability tests. The relative deviation for porosity determinations is 0.5%–1.5%
174 and that of permeability is ≤10% for low permeability samples.

RESULTS

Lithology, texture, and depositional characteristic

Lithology of the Xiaohaizi Formation in the study area comprises of calcitic marlstone, marly limestone, lime grainstone, partly dolomitized limestone and dolostones. There are two members of the Xiaohaizi Formation (Fig.2). The lithology of the upper member is dominantly argillaceous, marly limestone containing a very small amount of biodetritus and terrigenous siliciclastic grains. Marly limestone of the upper member deposited in the lagoon on a carbonate platform. In contrast, the lower member are characterised by granular dolostones and limestones, depositing on carbonate shoals. Besides the granular dolostone, the dolomicrite are observed in the interval. These dolomicrite composed of microcrystalline dolomites, occasionally with algal laminae, which deposited in the subtidal zone under a restricted marine environment.

Oil-bearing reservoirs are mainly composed of partly dolomitized limestones and granular dolostones in the lower member. These carbonate rocks are impure with a small amount of terrigenous detrital sands dominating by quartz. The content of terrigenous sands accounts for up to 10 vol. % of whole rock framework under microscope, occasionally 15 vol. % (Table 2). The composition of minerals determined by XRD shows that kaolinite accounts for 1-6 wt. % (Table 3). In addition, there is a small amount of pyrite.

196 The main textures of granular limestones are of grain-supported. The white
197 limestones, with grain-supported texture are represented by intrasparite limestones,
198 biosparite limestones and oospartie limestones. These carbonate rocks contain a wide
199 array of bioclastic material including fusulinid, foraminifera, brachiopod, bivalve,
200 echinodermata, and so on (Fig.3). The oncoids occasionally occurred within
201 intraclastic limestones. The kernels of oncoids and ooids include the bivalve debris,
202 echinodermata debris, and even quartz (Fig.3). These granular limestones deposited in
203 different shoals, including intraclastic shoals, bioclastic shoals, and oolitic shoals. The
204 dolomitization of grains is pervasive in limestones of intraclastic shoals and bioclastic
205 shoals, resulting in the formation of partly dolomitized intrasparite/ biosparite
206 limestones and finely crystalline granular dolostones. The crystal of dolomite is dirty
207 and fine (Fig.3). The textures of granular dolostones are of grain-supported, but with
208 the residual grain fabric and dark earthy yellow colour. The dissolved pores and vugs
209 can be observed in the grain-supported dolostones. There are several discrete layers of
210 dolostones alternating with undolomitized limestone at the lower member of the
211 Xiaohaizi Formation (Fig.2). As a result, the lithologic heterogeneity occurs in the
212 Xiaohaizi Formation.

213 The petrography of the granular dolostones shows some subaerial exposure
214 features, including percolating clay, vadose silt, palaeosol, and karst breccia (Fig.4).
215 The greyish-green percolating clay can be observed on cores. These percolating clays
216 also can be seen under microscope. A very small amount of vadose silt filled in the
217 moldic pores of biodetritus (Fig.4a), and karst breccia occurred in thin sections of well

218 BT8 (Fig.4b). The vadose silts have dark color, might be dyed by organic matters.
219 The palaeosol as the weathering product occurred on cores from well BT3 (Fig.4c).
220 The color of palaeosol was greyish-green, result from reduction during the diagenesis.
221 The terrigenous elements enriched in dolostones adjacent to palaeosol layer, in terms
222 of the concentration of terrigenous elements (Table 4).

223 ## *Diagenetic Minerals*

224 **Calcite.**-Calcite is the most abundant cement in the Xiaohaizi Formation. There
225 are two generations of calcite cementation identified in sparry allochemical
226 limestones (Fig.5). Based on the observation of thin sections, the first generation of
227 calcite cementation occurs mainly as bladed calcite forming isopachous fringes on
228 grains. The colour of bladed calcites under CL is dull, which is darker than the colour
229 of grains (Fig.3ab). The second generation is of blocky spar, filling in the
230 intergranular space (Fig.3c). The colour of blocky spar under CL is weak orange
231 (Fig.3d). After alizarin Red and potassium ferricyanide staining, the colour of blocky
232 calcite mostly becomes red, with very few mauve. The mauve colour shows the
233 blocky spar comprised of a small amount of ferroan calcite.

234 The poikilotopic texture developed in granular dolostones, rather than the two
235 generations of calcite cementation. Some partly dissolved dolomite crystals were
236 embedded in poikilotopic calcites. The colours of poikilotopic calcites under CL are
237 dull or dark orange (Fig.3d).

238 Micro-fractures are observed in biosparites and intrasparites, with two phases of
239 calcite filling. The early calcites filled in the micro-fractures have bright orange CL

240 colours, while the late calcites have very dark orange CL colours (Fig.3ef). In addition,
241 the neomorphic calcites filled within bivalve's debris (Fig.3e).

242 **Dolomite.**-The dolomitization in the Xiaohaizi Formation resulted in the
243 formation of micritic dolostones, partly dolomitized biosparite/intrasparite limestones,
244 granular dolostones (Fig.5). The dolomite crystals of biogenic dolostones and
245 intraclastic dolostones are euhedral, comprising of cloudy crystals with earthy yellow
246 colour under plane-polarized light (Fig.5eg). Under CL, the colours of dolomites in
247 these dolostones are dark red. The dolomitization of grains in granular dolostones is
248 nearly complete, comprised of dolomitized grains and poikilotopic calcite cements.
249 The dark earthy yellow colour of dolostones might be related to exposure, for the
250 organic matter detected on the surface of dolomite (Fig.5h). The CL colours of
251 dolomitized grains are dull (Fig.5e), implies different mechanisms with that of partly
252 dolomitized grains. In addition, micritic dolomites as matrix are observed, with weak
253 red CL colours (Fig.5).

254 **Kaolinite and dickite.**-Kaolinite and dickite are frequently observed in granular
255 dolostones and limestones of the Xiaohaizi Formation. Kaolinite could form by
256 chemical weathering or hydrothermal alteration of aluminosilicate minerals (Kerr
257 1952; Maliva et al. 1999). Blocky dickite is a polytype of kaolin, which can transform
258 from vermiform kaolinite (Bailey 1980; Ehrenberg et al. 1993). Based on the
259 observation of SEM, dickites have crystal size of 3-13μm (Fig.6a). The kaolinites or
260 dickites distribute in the intergranular pores, dissolved pores (Fig.6a), intercrystalline
261 pores of dolomite, and dissolved segment of stylolite. The CL colours of kaolinite and

dickite are deep blue (Fig.6d). The identification of dickite by X-ray diffraction was published on our previous study (Fu et al. 2012b).

Fluorite.-A small amount of fluorite, mostly less than 1 vol. %, was observed in the dolostones from the Xiaohaizi Formation in well BT3, M4 and BT4 (Fig.6eg). Although the fluorite has not detected by XRD, there are a few fluorites in the sample from well BT4 at 4312.11m, with 2-3 vol. % of whole rock. The paradox is caused by the different samples with the same depth were tested by XRD and observed under microscope. Fluorites filled in the dissolved pores and micro-fractures, even growing as a euhedral crystal (Fig.6ef). Through observation under CL, the fluorites have bluish-violet CL colours, while some residual dissolved dolomites enclosed by the fluorite crystal (Fig.6g). In some thin sections, fluorite and dickites synchronously existed in dissolved pores (Fu et al. 2012b) (Fig.6g).

Pyrite.-Authigenic pyrite is occasionally observed in dolostones from the Xiaohaizi Formation. There is small amount of authigenic pyrites in well BT4 at 4312.11m under microscope (Fig.6h). However, the abundance of pyrite tested by XRD (see Table 3) is different with the result observed under microscope, which is caused by the different sample with the same depth. Using energy spectrum identification, authigenic pyrites filled in a large number of dissolved pores (Fig.6h). It implies that the authigenic pyrite postdating the late dissolution.

Overgrowth quartz.-The terrigenous quartz has experienced diagenetic alteration, including replacement, compaction/pressure dissolution and overgrowth. Overgrowth quartz was frequently observed in the porous dolostones containing fluorites and

dickites. There were fine crystals of dolomite existing between detrital quartz and overgrowth quartz (Fig.6i). In sparry allochemical limestones, quartzes were prone to overgrows as euhedral crystal, while quartzes overgrew towards pores in porous dolostones.

Anhydrite/Gypsum.-Anhydrite or gypsum with plate like structure and bright interference colour occasionally can be observed in few samples, e.g. from well BT6 and BT8 (Fig.6j). The amount of anhydrite or gypsum is very few, only with less than 1 vol. % of whole rocks in two samples.

Carbon and oxygen stable isotope

The $\delta^{18}O_{\text{-carbonate}}$ of bulk carbonate ranges from -7.9‰ to 0.2‰PDB (Fig.7). There was an enrichment of ^{18}O during the global cooling in the Late Carboniferous-Permian (Veizer et al. 1999). There is an obvious vertical variation of $\delta^{18}O_{\text{-carbonate}}$ of Xiaohaizi Formation in well M10, might being related to the glacio-eustatic fluctuation. The shrift of dolostones to sparry allochemical limestones results in a 0.2‰ shift to more depleted $\delta^{18}O$ values of -7.4‰, as the boundary of glaciation and interglaciation (Fig.7). Meanwhile, the $\delta^{13}C$ values shift from -0.2‰ to 2.9‰ (Fig.7). There is obvious decrease of $\delta^{13}C$ values with $\delta^{18}O$ values.

Dissolution

The limestones and dolostones have experienced different phases of dissolution. There were three phases of dissolution. The first phase was the fabric selective dissolution, resulting in the formation of intragranular dissolved pores (Fig.8a). The

second phase was the non-fabric selective dissolution. The dissolved pore was completely filled with blocky calcite (Fig.8b). The third one was the late dissolution, with development of intergranular dissolved pores and intercrystalline dissolved pore of dolomite without fillings (Fig.8c). Occasionally, dissolution of feldspar can be observed (Fig.8c). Dissolution gave rise to the generation of abundant pores in intraclastic or biogenic dolostones, creating a complicated pore network. There are also some intergranular pores observed in the granular dolostones and limstones without or very weak cementation (Fig.8d).

Physical properties

The lithologic heterogeneity results in various pore assemblies in carbonate reservoirs of the Xiaohaizi Formation. The lime grainstones, e.g. biosparite limestones and intrasparite limestones, generally have few visible pores (Fig.8). The two generations of calcite cements almost obstructed intergranular pores. The dissolved fractures and early non-fabric selective dissolved pores were fully filled with calcite (Fig.3). Few unfilled intergranular pores and intragranular pores developed in the granular limestones result in low porosity and permeability, with 0.4-2.5%, and 0.00-0.62mD, respectively (Fig.9). However, intrasparite limestones without cementation of blocky calcites (Fig.8d) have relative high porosity and permeability, with 8.5-14.8% and 5.33-39.5mD, respectively (Fig.9).

Dolostones develop more visible pores than limestones. Even so, the amount of pores in dolostones depends on the degree of dolomitization and cementation. The pores in dolostones are characterised by intergranular pores, intercrystalline pores,

and dissolved pores. The partly dolomitized limestones with low degree of dolomitization have relative lower porosity and permeability than dolostones (2.5-5.8%, 0.01-2.16mD) (Fig.9). The porosity of dolostone was obviously influenced by poikilotopic calcite cementation. The dolostones without poikilotopic calcite have porosity of up to 16.6%, and permeability of up to 214mD (Fig.9).

DISCUSSION

Sedimentation on a mixed siliciclastic-carbonate platform

There are two sedimentary environments developed during the deposition of the Xiaohaizi Formation, including lagoon and carbonate shoals on a mixed siliciclastic-carbonate platform. As shown in Figure 2, the sedimentary environment of the Xiaohaizi Formation gradually changes from carbonate shoals to lagoon. The comparison among reservoir quality of rocks from different sedimentary facies is shown in Table 5. Marl limestones deposited in the lagoon with low hydrodynamic force are non-reservoir lithofacies. Within marl limestones, marl is the main element, with very few biodetritus and terrigenous detrital grains probably transported by storm waves. The pores within marl limestones were missing under microscope. Except the marl limestones with none visible porosity, the reservoir rocks deposited on the carbonate shoals include granular limestones, partly dolomitized limestones and granular dolostones. In terms of the physical properties of these rocks from the Xiaohaizi Formation, granular limestones with two generations of calcite cementation have fewest porosity than other three rocks (Fig.9). Some intraclastic limestones have

only one generation of cementation, with more pores (Fig.8d). The partly or complete dolomitization in original biogenic limestones and intraclastic limestones results in the formation of porous dolostones reservoir, while there is no dolomitization observed in original oospartie limestones. Sum up, the reservoir rocks deposited on intraclastic shoals and biogenic shoals usually have a wide range from very poor to good physical properties (Table 5). The heterogeneity of physical properties comes from different diagenetic process (e.g. calcite cementation and dolomitization). However, the limestones deposited on oolitic shoals are always to be poor reservoirs. In addition, dolomicrite deposited on subtidal zone around shoals has low porosity with a very small amount of intercrystalline pores.

In terms of the observation and geochemical composition, there are a small amount of terrigenous siliciclastic grains and clay minerals inputting into the carbonate shoals (Table 2, 3, 4). In our previous study, the size distribution of quartz particles in the Xiaohaizi Formation shows the terrigenous materials deposited on the mixed carbonate shoals came from beach sands or aeolian sands (Fu et al. 2011). The siliciclast could be transported into carbonate platform by wind and current during mixed siliciclastic-carbonate sedimentation (Mount 1984; Fay et al. 1992; Brandano and Civitelli 2007). According to Fig.10a，the detrital quartz grains are prone to occur together with biodetritus (dominated by fusulinid and foraminifera) in sparry granular limestones (Table 2, Fig.10a). However, the contents of quartz within granular dolostone are relatively high, with up to 8% (Fig.7). The complete dolomitized grains in granular dolostones almost were the original intraclastic grains. It’s probably that

there was relatively abundant quartz within original intraclastic limestones. Comparing with biodetritus and intraclast, the deposition environments of ooids and oncoids grains are little influenced by mixed siliciclastic-carbonate sedimentation. According to the content of terrigenous detrital quartz, the sedimentary facies on a mixed carbonate platform could be divided into mixed bioclastic and intraclastic shoals and normal shoals. The bioclastic and intraclastic shoals influenced by mixed sedimentation are proved to have highly reservoir quality with evidence from figure 10b.

The mixed sedimentation on the carbonate shoals could influence the physical property of reservoirs. The contents of terrigenous detrital quartz within carbonate rocks have a good positive relationship with their porosities (Fig.10c). In this study, the mixed sedimentation was regarded as the response to the glacio-eustatic fluctuations. There is a good correlation between content of detrital quartz and $\delta^{18}O_{\text{-carbonate}}$, as shown in Fig.7. Due to there was an enrichment of ^{18}O during the global cooling (Veizer et al. 1999), the increase of $\delta^{18}O_{\text{-carbonate}}$ verifies the onset of a glacial period. With the enhancement of glacial period, the sea level declined and the subaerial emergence occurred, with more input of terrigenous materials. The leaching of carbonate rocks by meteoric water during subaerial emergence could improve the physical property of reservoirs. Therefore, the mixed sedimentation related to glacio-eustatic fluctuations is an important factor controlling reservoir quality.

Diagenetic processes and subaerial diagenesis related to glacio-eustatic fluctuations

The diagenetic process of carbonate rocks from the Xiaohaizi Formation was established (Fig.11). The main diagenetic factors that influenced the reservoir quality include calcite cementation, subaerial exposure influenced by meteoric water, diagenesis related to hydrothermal fluid and dolomitization, as well as quartz overgrowth (Table 6). The effects of these diagenetic alterations on reservoir quality have been compared in Table 6. The dolomitization and dissolution related to meteoric water and hydrothermal fluid were the upmost important constructive diagenetic alteration, while calcite cementation destroyed the physical property.

There are different paths of paragenesis for sparry allochemical limestones and granular dolostones in the Xiaohaizi Formation (Fig.11). The cements of bladed high-magnesium calcite with dull CL colour around allochems and the framboidal pyrite occurred during early marine diagenesis. Under early diagenesis conditions, dolomitization of allochems predated the precipitation of bladed high-magnesium calcite. For complete dolomitized allochems, bladed calcite cements are absent. For the non-dolomitized limestone, the precipitation of blocky spars postdated the bladed cements to generate two phases of calcite cements. The two phases of calcite cements destructed the intergranular space among particles, resulting in the lowest porosity among granular limestones.

With evidence from petrography of dolostones and $\delta^{18}O_{\text{-carbonate}}$ of bulk carbonate analysis we can be sure that the diagenetic processes occurred during subaerial

412 exposure, resulting from the glacio-eustatic sea level changes in the Late
413 Carboniferous. During the sea-level fall as the result of glaciation with low CO_2,
414 palaeosol formed after weathering of limestone and micritic carbonate minerals, and
415 vadose silt filled in few pores during the subaerial exposure (Fig.4). The similar
416 diagenetic alteration is reported elsewhere (Butts 2005; Ueno et al. 2013). In addition,
417 granular dolostones have dark earthy yellow colours. The origin of the dark colour
418 might be related to organic matter during exposure (Fig.6h) (Ueno et al. 2013). In the
419 other hand, based on the vertical variation of $\delta^{18}O_{\text{-carbonate}}$, the positive apexes of $\delta^{18}O$
420 could represent the cold intervals during the glaciations (Fig.7). According to the
421 fractionation of oxygen isotope, large amounts of ^{16}O water are being stored as glacial
422 ice (Veizer et al. 1999). The generation of ice caps could have been the principal
423 reasons for the observed ^{18}O enrichments. The upward trend to relative positive $\delta^{18}O$
424 values from interglaciation to glaciation in this study could be interpreted as a signal
425 of long-term increase in salinity, being similar with the study of Mazzullo et al.
426 (2007). There are some similar high frequency, moderate amplitude fluctuations in sea
427 level during different periods when the globe is transitional between ice-house and
428 green-house conditions, e.g. the Early/Late Ordovician, Early/Late Carboniferous
429 boundary, Early/Late Permian boundary and parts of the early Neogene (Read and
430 Horbury 1993).

431 However, the subaerial exposure of the lower member of the Xiaohaizi
432 Formation lacks meteoric diagenetic fabric (Fig.4). The meniscus and dripstone
433 cementation was absent. The lack of macro-scale karst or evidence of epidiagenesis

434 suggests relatively short-lived exposure and/or a dry climate (Choquette and James
435 1988). Non-fabric selective dissolution occasionally occurred under inefficient
436 meteoric diagenesis environment.

437 At the shallow burial process, dissolution occurred in porous dolostones
438 experienced a very weak cementation in the early diagenesis. It's suggested that the
439 composition of mineral during ice-house times was mainly of global aragonite and
440 high-Mg calcite (Sandberg1983), resulting in greater rates of early carbonate
441 dissoloution. As a result, a large number of dissolved pores generated to increase the
442 porosity further. After that, the pores without fillings in dolostones were partly filled
443 by poikilotopic calcites. The kaolinite and overgrowth quartz precipitated after the
444 feldspar dissolution. With particular hydrothermal fluid accumulated in porous
445 dolostones along faults in some areas, authigenic minerals formed, e.g. fluorite,
446 dickite and authigenic pyrite precipitated, as well as quartz overgrowth. Finally, with
447 the oil charging, the diagenesis mostly ceased.

448 ***Occurrence and origin of kaolinite and dickite***

449 The occurrence of authigenic kaolinite and dickite in carbonate rocks is related to
450 chemical weathering, diagenesis, or hydrothermal fluid alteration (Schroeder and
451 Hayes 1968; Jacka and Guven 1979; Maliva et al. 1999; Esteban and Taberner 2003;
452 Fu et al. 2012b; Liu et al. 2016).

453 The formation of kaolin in the Xiaohaizi Formation was related to the dissolution
454 of feldspar in the impure carbonate rocks, evidence from the petrography observation
455 (Fig.8). The mix sedimentation of siliciclastic and carbonate minerals resulted in the

456 input of terrigenous sands, including quartz, feldspar and lithic fragment. The
457 kaolinite could form through meteoric water leaching both plagioclases and
458 K-feldspars, under the subaerial environment, during early diagenesis or after
459 structural inversion (Lanson et al. 2002). As a consequence of feldspar dissolution,
460 kaolin precipitates according to:

461 $$2KAlSi_3O_8 + 2H^+ + 9H_2O \leftrightarrow Al_2Si_2O_5(OH)_4 + 4H_4SiO_4 + 2K^+ \quad (1)$$

462 Feldspar Kaolinite Silica

463 It's reported that there is a 5×10^6a depositional break at the end of Carboniferous
464 (Xiao et al. 1995). As discussed above, there was subaerial emergence inside the
465 Xiaohaizi Formation. However, the duration of exposure wouldn't last a long time.
466 Scarcity of meteoric diagenetic fabrics and the occasional occurrence of gypsum in
467 the study area indicate a less influence from meteoric water and a relative arid
468 environment, just like the study of Triassic platform carbonate in a low latitude,
469 tropical but arid setting (Christ et al. 2012). On the other hand, due to the amounts of
470 siliciclastic grains within granular limestones and granular dolostones are very small
471 (Table 2, 3), the input of feldspar during deposition period wouldn't be abundant. The
472 insufficient meteoric water and a small amount of feldspar input resulted in the
473 precipitation of kaolinite with content of less than 6% (Table 3). The detrital kaolinite
474 deposited with allochems as the product of chemical weathering.

475 There is another hypothesis for the origin of diagenetic kaolin. CO_2-rich or
476 organic acid-rich fluids may be responsible for feldspar alteration and subsequent
477 precipitation of kaolin in buried sandstone (Ehrenberg 1991; Gaupp et al. 1993).

Kaolin can precipitate from the organic-rich pore water in limestones during burial diagenesis (Schroeder and Hayes 1968; Esteban and Taberner 2003; Fu et al. 2012b). In this study, the occurrence of kaolinite and dickite and overgrowth quartz synchronously existed in the finely crystalline biogenic and intraclastic dolostones with high visible porosity. The overgrowth quartz developed towards pores (Fig.6i), indicating the silica was supersaturated in the pore water of the Xiaohaizi Formation. Due to the relative high solubility of aluminum in organic acid-rich pore water (Maliva et al. 1999), the aluminum can be released by feldspar dissolution. In the study area, there are at least two times of oil charging, while the early oil charging occurred at Permian related to the Late Hercynian orogeny (Shao et al. 2010; Wang et al. 2015; Song et al. 2018). The intrusion of organic-acid predating oil charging resulted in the dissolution of feldspar, the precipitation of kaolin and the overgrowth of quartz. The partly dissolution of feldspar can be observed in thin sections (Fig.8c). The precipitation of vermiform kaolinite is also likely to occur in the burial diagenesis, resulting from *in situ* organic-acid dissolution of feldspar.

Dickite in the Xiaohaizi Formation can form through two pathways of diagenetic alteration (Fig.12). The kaolinite converted to dickite with increasing burial temperature (Lanson et al. 1996; Beaufort et al. 1998; Lanson et al. 2002; De Bona et al. 2008). Dickitization is of temperature-dependence, occurring at 100~130°C (Ehrenberg et al. 1993). However, it's hard to explain the occurrence of dickite in well BT3 on the Bachu uplift with burial depth of 1944m, equivalent to 83 ºC (normal geothermal gradient 3 ºC/hm). According to the burial history of well BT4 in study

area (Wang et al. 2015), the maximum burial depth of the Xiaohaizi Formation wouldn't be more than the depth at present. The low temperature of 83 ºC is not enough to cause dickitization of kaolinite. The hydrothermal activity in the study area probably is responsible for the dickitization. The high water/rock ratio during hydrothermal fluid accumulation is beneficial to dickitization (Lanson et al. 2002). The fluorite, as an indicator for hydrothermal fluid (Davies and Smith 2006), was also observed in the samples containing dickite (Fig.6). As a result, dickite mostly precipitated from hydrothermal fluid rather than transforming from kaolinite.

The effect of hydrothermal fluid on dolostone reservoirs

During the Early and Middle Permian, ultrabasic dyke was found in Bachu area resulting from the volcanic and igneous activity in Tarim Basin (Yang et al. 2007). The hydrothermal fluid migrates upwards along faults with volcanic activity. Few similar studies discussed the effect of hydrothermal fluid on dolostone reservoirs of the Xiaohaizi Formation in the study area (Fu et al. 2011, 2012b; Ma et al. 2015). In this study, evidence from the assembly of dickite, fluorite and authigenic pyrite indicated there was hydrothermal fluid activity. Fluorite postdated the precipitation of dickite. Authigenic pyrite formed in the dissolved pores as the react product of hydrothermal fluid rich in Fe^{2+} and H_2S. Sulfur could come from the underlying strata containing abundant gypsum (Fig.1). The homogenization temperatures of saline inclusions bearing hydrocarbon within calcite veins in well BT4 have the maximum value of 152.4°C (Fig.13), showing there was a high temperature resulting from hydrothermal fluid in the late diagenesis. The accumulation of hydrothermal fluid

522 with high temperature and high water/rock ratio in dolostones could give rise to the
523 formation of numerous dissolved pores, improving the physical property of reservoirs.
524 Conversely, the precipitation of authentic minerals, e.g. fluorite, dickite, will fill with
525 pores to decrease the porosity.

526 In the study area, a small amount of fluorite (mostly less than 1 vol. %) might
527 imply the much less influence from hydrothermal fluid. The distribution of fluorite is
528 strictly controlled by hydrothermal fluid. The porosity of dolostones containing
529 fluorite is up to 13.5%, with average value of 9.7%. The abundant dissolved pores in
530 dolostones without fillings indicate the possibility of late dissolution caused by
531 hydrothermal fluid. The high primary porosity of dolostones facilitates the flow of
532 hydrothermal fluid. The effect of hydrothermal fluid on physical property of
533 dolostones with relative high primary porosity was positive.

534 However, the coarse crystalline poikilotopic calcite cements filled in pores of
535 dolostones might result from hydrothermal fluid accumulation. The CL colour of
536 poikilotopic calcite was dark orange (Fig.3bd), brighter than blocky calcite, showing a
537 relative high concentration of Mn^{2+} (Hiatt and Pufahl 2014). As we know, meteoric
538 water was the main source of manganese (Livingstone 1963). The input of Mn^{2+} has
539 two potential sources including meteoric water and hydrothermal fluid. As discussed
540 above, the arid palaeo-climate in the study area could result in less rainfall on the
541 carbonate platform, leading to inefficient meteoric water diagenesis. Therefore, the
542 high concentration of Mn^{2+} had relations with hydrothermal fluid rather than meteoric
543 water in the early diagenesis. Fe^{2+} can quench luminescence (Hiatt and Pufahl 2014)

544 to darken the luminescence. The precipitation of authentic pyrites could consume the
545 spare Fe^{2+} from hydrothermal fluid. As a result, the relative brighter luminescence
546 coarse crystalline poikilotopic calcite attributed to the relative high concentration of
547 Mn^{2+} from hydrothermal fluid. The cementation following hydrothermal fluid
548 accumulation could be the most deconstructive factor of physical property.

549 ***Dolomitization controls the reservoir quality***

550 The physical property of the Xiaohaizi Formation is mainly controlled by
551 dolomitization (as shown in Fig.9, Fig.10d). The earthy yellow dolomite crystals in
552 these dolostones with fabric-retentive texture are characterised by small size, cloudy
553 and euhedral-subhedral, with dark red colour under CL (Fig.5). The fabric-retentive
554 texture shows the dolomitization occurred in the early diagenesis under
555 low-temperature (Machel 2004). In this study, the porous dolostones alternated with
556 tight limestone, caused by different degrees of dolomitization. The degrees
557 dolomitization of allochems could be related to the surface-water circulation during
558 sedimentation, through seawater evaporation (Machel 2004).

559 The multiple phases of eustatic fluctuation occurred in the Late Carboniferous, as
560 the consequence of Gondwanan glaciation (Rygel et al. 2008; Buggisch et al. 2015).
561 A similar study from Yangtze carbonate platform (China) in the Late
562 Carboniferous-Early Permian, located in the similar palaeo-latitude with the study
563 area, indicates the marine transgression and regression resulting from variations in the
564 Gondwanan ice sheets (Ueno et al. 2013). The glacio-eustatic fluctuation caused the
565 episodical restricted environment on carbonate shoals. In the restricted environment,

566 the evaporation of active reflux brines can generate the mesohaline brines. However,
567 seawater was below gypsum saturation during most of the complete dolomitization for
568 the absence of gypsum precipitated in the study. The less negative δ^{13}C of whole
569 carbonate rocks excludes the microbial or organogenic model of dolomitization. The
570 darkening of dolostones also supports the subaerial emergence (Ueno et al. 2013).
571 Although the mechanism of dolomitization is mysterious, we suggest that the change
572 of sedimentary environment caused by glacio-eustatic fluctuation controlled the
573 complete dolomitization during penecontemporaneous period.

574 Based on the petrography, the partial dolomitized grains were enclosed by
575 isopachous bladed calcite, with brighter CL colour (Fig.5b,d) than completely
576 dolomitized grains (Fig.5f). The formation of partial dolomitized grains might have
577 another mechanism. Similar study speculated the reflux of gypsum-saturated brines
578 could form discrete layers of dolostone that alternating with undolomitized limestone
579 (Jones et al. 2003). The paragenesis represents a continuum of diagenetic processes
580 resulting from progressive modification of diagenetic fluids. It's credible that the
581 latent reflux brines were responsible for the partial dolomitization at shallow burial
582 stage, for the rare anhydrite occurred in the partly dolomitized intrasparite (Fig.6J).

583 *Control of glacio-eustatic fluctuations on mixed sedimentation and*
584 *diagenesis in carbonates and implications for forecasting reservoir*
585 *quality*

586 The mixed sedimentation and diagenetic processes inferred from petrographic
587 observations and isotope analysis of the Xiaohaizi Formation are clearly linked to the

588 glacio-eustatic conditions that existed in the area of what is now the Tarim Basin in
589 the Late Carboniferous. The correlation between the content of terrigenous detrital
590 quartz and $\delta^{18}O_{\text{-carbonate}}$, together with petrographic features under subaerial emergence,
591 show the coincidence of sea level fall and mixed sedimentation. The granular
592 dolostones deposited on mixed carbonate shoals have higher porosities than granular
593 limestone on normal shoals. The suit of diagenetic minerals to occur as well as the
594 absence of evidence for components like drip stones in these carbonate deposits
595 indicates the importance of the predominantly cold, arid conditions during the
596 exposure period (Read and Horbury 1993). It's clear that the reservoir quality of
597 carbonate rocks in the Xiaohaizi Formation under cold and arid conditions was
598 controlled by the mixed sedimentation and early diagenesis, especially dolomitization
599 and weak cementation, as response to the sea level fall during glacial period. The
600 depositional and diagenetic model of the Xiaohaizi Formation was established
601 (Fig.14).

602 The limitations of this work stem principally from it being focused on a single
603 basin in western China. It seems likely that carbonate strata of similar age in different
604 locations around the globe should show some of the characteristic linked to sub-aerial
605 exposure although it is likely that other locations will give an indication of humid
606 rather than arid conditions. Further work on similar age carbonate sequences
607 elsewhere in the world should enable a comprehensive understanding to be developed
608 of the contemporaneous climate and sea-level conditions during the late
609 Carboniferous. Moreover, given the impact the digenetic processes have had on

improving reservoir quality in these carbonates, it should be possible once data from other basins are assembled, to construct a method whereby the quality of carbonate reservoir from the Late Carboniferous can be forecasted. This would be of significant value to both the petroleum and geothermal industries.

CONCLUSION

The reservoir quality of the Xiaohaizi Formation was controlled by mixed siliciclastic-carbonate sedimentation and dolomitization as response to glacio-eustatic fluctuation in the Late Carboniferous, with the contribution from subaerial exposure and partly from hydrothermal fluid alteration.

The lithology of the Xiaohaizi Formation gradually changes from granular limestones and dolostones deposited on carbonate shoals to marl limestones of lagoon. Discrete layers of porous dolostones alternating with tight undolomitized limestone within the shoal facies. It's suggested that the mixed sedimentation could affect the reservoir quality, with evidence from the positive correlation between the content of terrigenous quartz and porosities of carbonate rocks. During glacial period, mixed sedimentation resulted in dolostones deposited on mixed shoals having higher porosities than that on normal shoals.

The dolostones have middle-high porosity and permeability, with maximum values of 16.6%, 214mD, respectively. The dolomitization of grains formed under low-temperature, which was related to episodical restricted environment. It's clear that penecontemporaneous dolomitization and weak cementation controlled the reservoir quality, during subaerial exposure period. Evidences for the emergence of

632 dolostones include vadose silt. palaeosol, karst breccia, detrital kaolinite, darkening of
633 dolostones, and positive $\delta^{18}O_{\text{-carbonate}}$.

634 The contribution of hydrothermal fluid to the reservoir quality in the burial
635 diagenesis was positive, although resulting in some poikilotopic calcite cementation.
636 The assembly of fluorite, dickite and antigenic pyrite was the indicator of
637 hydrothermal fluid accumulation. The dickite precipitated from hydrothermal fluid as
638 the react product of feldspar dissolution under high temperature.

639 # ACKNOWLEDGEMENTS

640 We thank Professor Huang Si-jing from Chengdu University of Technology for his
641 constructive suggestion. We thank SinoPec of China for providing rock samples. We
642 thank the State Key Laboratory of Oil and Gas Reservoir Geology and Exploitation in
643 China for the measurement. The financial support of the research comes from the
644 National Natural Science Foundation of China (Grant No. 41402096).

645 # REFERENCES

646 Bailey, S.W., 1980. Structures of layer silicates, *in* Brindley, G. W. & Brown, G., eds.,
647 Crystal structures of clay mineral and their X-ray Identification: Monograph 5,
648 Mineralogical Society, London, p. 1-123.

649 Beaufort, D., Cassagnabère, A., Petit, S., et al., 1998, Kaolinite-to-dickite conversion
650 series in sandstone reservoirs: Clay Minerals, v. 33, p. 297-316.

651 Bishop, J. W., Montanez, I. P., Gulbranson, E.L., et al., 2009, The onset of
652 mid-Carboniferous glacio-eustasy: Sedimentologic and diagenetic constraints, Arrow

653 Canyon, Nevada: Palaeogeography, Palaeoclimatology, Palaeoecology, v. 276.1, p.
654 217-243.
655 Brandano, M., and Civitelli, G., 2007, Non-seagrass meadow sedimentary facies of
656 the Pontinian Islands, Tyrrhenian Sea: a modern example of mixed
657 carbonate–siliciclastic sedimentation: Sedimentary Geology, v. 201.3, p. 286-301.
658 Buggisch, W., Krainer, K., Schaffhauser, M., et al., 2015, Late Carboniferous to Late
659 Permian carbon isotope stratigraphy: A new record from post-Variscan carbonates
660 from the Southern Alps (Austria and Italy): Palaeogeography, Palaeoclimatology,
661 Palaeoecology, v. 433, p. 174-190.
662 Butts, S. H., 2005, Latest Chesterian (Carboniferous) initiation of Gondwanan
663 glaciation recorded in facies stacking patterns and brachiopod paleocommunities of
664 the Antler foreland basin, Idaho: Palaeogeography, Palaeoclimatology, Palaeoecology,
665 v. 223.3, p. 275-289.
666 Choquette, P. W., James, N. P., 1988, Introduction, *in* James, N.P. and Choquette,
667 P.W., eds., Paleokarst: Springer-Verlag, New York, p. 1–24.
668 Christ, N., Immenhauser, A., Amour, F., et al. 2012, Triassic Latemar cycle
669 tops-Subaerial exposure of platform carbonates under tropical arid climate:
670 Sedimentary Geology, v. 265, p. 1-29.
671 Crowley, T. J., and Baum, S. K., 1991, Estimating Carboniferous sea-level
672 fluctuations from Gondwanan ice extent: Geology, v. 19.10, p. 975-977.
673 Davies, G. R. and Smith, J. L. B., 2006, Structurally controlled hydrothermal dolomite
674 reservoir facies: an overview: AAPG Bulletin, v. 90, p. 1641–1690.

De Bona, J., Dani, N., Ketzer, J. M., et al., 2008, Dickite in shallow oil reservoirs from Recôncavo Basin, Brazil: diagenetic implications for basin evolution: Clay Minerals, v. 43.2, p. 213-233.

Ehrenberg, S. N., 1991, Kaolinized, potassium-leached zones at the contacts of the Garn Formation, Haltenbanken, mid-Norwegian continental shelf: Marine Petroleum Geology, v. 8, p. 250-269.

Ehrenberg, S. N., Aagaard, P., Wilson, M. J., et al., 1993, Depth-dependent transformation of kaolinite to dickite in sandstones of the Norwegian Continental shelf: Clay mineral, v. 28, p. 325-352.

Elrick, M., and Scott, L. A., 2010, Carbon and oxygen isotope evidence for high-frequency (10 4–105yr) and My-scale glacio-eustasy in Middle Pennsylvanian cyclic carbonates (Gray Mesa Formation), central New Mexico: Palaeogeography, Palaeoclimatology, Palaeoecology, v. 285.3, p. 307-320.

Ernst, R. E. and Buchan, K. L., 2001, Large mafic magmatic events through time and links to mantle-plume heads, *in* Ernst, R.E. and Buchan, K.L., eds., Mantle Plumes: Their Identification Through Time. Geological Society of America Special Paper 352, p. 483–575.

Esteban, M., and Taberner, C., 2003, Secondary porosity development during late burial in carbonate reservoirs as a result of mixing and/or cooling of brines: Journal of Geochemical Exploration, v. 78, p. 355-359.

695 FAY, M., MASALU, D. C. P., MUZUKA, A. N. N., 1992, Siliciclastic—carbonate
696 transitions in surface sediments of a back-reef lagoon north of Dar es Salaam
697 (Tanzania): Sedimentary Geology, v. 78.1-2, p. 49-57.
698 FU, M. and ZHANG, S., 2011, Diagenesis of Quartz in Mixed Clastic-carbonate Rock
699 and Its Relationship with Reservoir: Journal of Oil and Gas Technology, v. 33.12, p.
700 50-54 (Chinese, Abstract in English).
701 FU, M., ZHANG, S., ZHAO, X., et al., 2012a, Researches of mixed sedimentation of the
702 Carboniferous in Bachu-Makit area in Tarim Basin: Journal of Palaeogeography, v.
703 14.2, p. 155-164 (Chinese, Abstract in English).
704 FU, M., ZHANG, S., HU, W., 2012b, The distribution and origin of dickite in carbonate:
705 Acta Sedimentologica Sinica, v. 30.2, p. 310-317 (Chinese, Abstract in English).
706 GAUPP, R., MATTER, A., PLATT, J., 1993, Diagenesis and fluid evolution of deeply buried
707 Permian (Rotliegende) gas reservoir, Northwest Germany: AAPG Bulletin, v. 77, p.
708 1111-1128.
709 HIATT, E. E., and PUFAHL, P. K., 2014, Cathodoluminescence petrography of carbonate
710 rocks: a review of applications for understanding diagenesis, reservoir quality, and
711 pore system evolution: Mineralogical Association of Canada, Short Course 45,
712 Fredericton, New Brunswick, p. 75–96.
713 JACKA, A. D., and GUVEN, N., 1979, Occlusion of Porosity in Carbonate Reservoirs by
714 Dickite: ABSTRACT: AAPG Bulletin, v. 63.3, p. 474-474.

715 JANNOT, Y. and LASSEUX, D., 2012, A new quasi-steady method to measure gas
716 permeability of weakly permeable porous media. Review of Scientific Instruments, v.
717 8, p. 2015-2113.
718 JIA, C., 2013, Characteristics of Chinese petroleum geology: geological features and
719 exploration cases of stratigraphic, foreland and deep formation traps: Springer Science
720 & Business Media. p.15.
721 JIANG, L. and GU, J., 2002, Analysis on the sedimentary environment of the
722 carboniferous carbonate and detrital rock alternating sedimentation in the Maigaiti
723 slope of the Tarim basin: Petroleum Geology & Experiment, v. 24.1, p. 41-47
724 (Chinese, Abstract in English).
725 JIANG, L., YU, D., 2003, Research on Reservoir Characteristics of Carboniferous
726 bioclast limestone member in Maigaiti Slope, Tarim Basin: Acta Scicentiarum
727 Naturalum Universitis Pekinesis, v. 39.3, p. 428 - 434 (Chinese, Abstract in English).
728 JONES, G. D., SMART, P. L., WHITAKER, F. F., et al., 2003, Numerical modeling of reflux
729 dolomitization in the Grosmont platform complex (Upper Devonian), Western Canada
730 Sedimentary Basin: AAPG Bulletin, v. 87, p. 1273–1298.
731 KERR, P. F., 1952, Formation and occurrence of clay minerals: Clays and Clay
732 Minerals, v.1.1, p. 19-32.
733 KORDI, M., MORAD, S., TURNER, B., et al., 2017, Sequence stratigraphic controls on
734 formation of dolomite: Insights from the Carboniferous Um Bogma Formation,
735 Sinai-Egypt: Journal of Petroleum Science and Engineering, v. 149, p. 531-539.

LANSON, B., BEAUFORT, D., BERGER, G., et al., 1996, Late-stage diagenesis of clay minerals in porous rocks: Lower Permian Rotliegendes reservoir off-shore of The Netherlands: Journal of Sedimentary Research, v. 66, p. 501-518.

LANSON, B., BEAUFORT, D., BERGER, G., et al., 2002, Authigenic kaolin and illitic minerals during burial diagenesis of sandstones: a review: Clay Minerals, v. 37, p. 1–22.

LI, D., LIANG, D., JIA, C., WANG, G., WU, Q., HE, D., 1996, Hydrocarbons accumulations in the Tarim Basin, China: AAPG Bulletin, v. 80, p. 1587–1603.

LI, Z., CHEN, H., SONG, B., et al., 2011, Temporal evolution of the Permian large igneous province in Tarim Basin in northwestern China: Journal of Asian Earth Sciences, v. 42.5, p. 917-927.

LI, Y., WEN, L., YANG, H., et al., 2015, New discovery and geological significance of Late Silurian–Carboniferous extensional structures in Tarim Basin: Journal of Asian Earth Sciences, v.98, p. 304-319.

LIU, L. H., MA, Y. S., LIU, B., et al., 2016, Hydrothermal dissolution of Ordovician carbonates rocks and its dissolution mechanism in Tarim Basin, China: Carbonates and Evaporites, p. 1-13.

LIVINGSTONE, D. A., 1963, Chemical composition of rivers and lakes, *in* Fleischer, M. eds., Data of Geochemistry: USA Reston Virgina, p. 41−44.

LÓPEZ-GAMUNDÍ, O. R., and BUATOIS, L. A., 2010, Introduction: Late Paleozoic glacial events and postglacial transgressions in Gondwana: Geological Society of America Special Papers, 468, v-viii.

758 Ma, Z., Yang, S., Xu, Q., et al., 2015, Main controlling factors of carbonate reservoirs
759 of Xiaohaizi Formation in Xianbazha area, Tarim Basin: Petroleum Geology &
760 Experiment, v. 37.3, p. 300-327 (Chinese, Abstract in English).
761 Machel, H. G., 2004, Concepts and models of dolomitization: a critical reappraisal:
762 Geological Society, London, Special Publications, v. 235.1, p. 7-63.
763 Maliva, R. G., Dickson, J. A. D., and Fallick, A. E., 1999, Kaolin cements in
764 limestones: potential indicators of organic-rich pore waters during diagenesis: Journal
765 of Sedimentary Research, v. 69, p. 158-163.
766 Maynard, J. R., and Leeder, M. R., 1992, On the periodicity and magnitude of Late
767 Carboniferous glacio-eustatie sea-level changes: Journal of the Geological Society, v.
768 149.3, p. 303-311.
769 Mazzullo, S. J., Boardman, D. R., Grossman, E. L., et al., 2007, Oxygen-carbon
770 isotope stratigraphy of Upper Carboniferous to Lower Permian marine deposits in
771 Midcontinent USA (Kansas and ne Oklahoma): Implications for sea water chemistry
772 and depositional cyclicity: Carbonates and Evaporites, v. 22.1, p. 55-72.
773 Mckay, J. L., Longstaffe, F. J., and Plint, A. G., 1995, Early diagenesis and its
774 relationship to depositional environment and relative sea‐level fluctuations (Upper
775 Cretaceous Marshybank Formation, Alberta and British Columbia): Sedimentology, v.
776 42.1, p. 161-190.
777 Meng, Q., Zhu, D., Xie, Q., et al., 2011, Controlling factors for deep fluid activity and
778 prediction of positive effect area in middle Tarim and Bachu region: Petroleum
779 Geology &Experiment, v. 33.6, p. 597-606.

780 MORAD, S., KETZER, J. M., DE ROS, L. F., 2012, Linking Diagenesis to Sequence
781 Stratigraphy: An Integrated Tool for Understanding and Predicting Reservoir Quality
782 Distribution, *in* MORAD, S., KETZER, J. M., DE ROS, L. F., eds., Linking
783 Diagenesis to Sequence Stratigraphy. International Association of Sedimentologists,
784 Special Publication, v. 45, p. 1–36.
785 MOUNT, J. F., 1984, Mixing of siliciclastic and carbonate sediments in shallow shelf
786 environments: Geology, v. 12, p. 432-435.
787 QING, H., BOSENCE, D. W. J., and ROSE, E. P. F., 2001, Dolomitization by penesaline
788 sea water in Early Jurassic peritidal platform carbonates, Gibraltar, western
789 Mediterranean: Sedimentology, v. 48.1, p. 153-163.
790 READ, J.F., and HORBURY, A.D., 1993, Eustatic and tectonic controls on porosity
791 evolution beneath sequence-bounding unconformities and parasequences
792 disconformities on carbonate platforms. *in* HORBURY, A.D., and ROBINSON, A.G.,
793 eds., Diagenesis and basin development, American Association of Petroelum
794 Geologists Studies in Geology #36, p. 155-197.
795 REN, M., and JONES, B., 2016, Diagenesis in limestone-dolostone successions after 1
796 million years of rapid sea-level fluctuations: A case study from Grand Cayman,
797 British West Indies: Sedimentary Geology, v. 342, p. 15-30.
798 RYGEL, M. C., FIELDING, C. R., FRANK, T. D., et al., 2008, The magnitude of Late
799 Paleozoic glacio-eustatic fluctuations: a synthesis: Journal of Sedimentary Research, v.
800 78.8, p. 500-511.

SANDBERG, P.A., 1983, An oscillating trend in Phanerozoic non-skeletal carbonate mineralogy: Nature, v. 305, p. 19-22.

SCHROEDER, R. J., and HAYES, J. B., 1968, Dickite and kaolinite in Pennsylvanian limestones of southeastern Kansas: Clays and Clay Minerals, v. 16, p. 41-49.

SCOTESE, C. R., and MCKERROW W. S., 1990, Revised world maps and introduction: Geological Society, London, Memoirs, v. 12.1, p. 1-21.

SHAO, Z., LV, H., and GENG, F., 2010, Geochemical characteristics of the Carboniferous oil pools in Maigaiti area, the Tarim Basin: Oil & Gas Geology, v. 31.1, p. 84-90 (Chinese, Abstract in English).

SONG, D., SHI, L. S. HAN, Z. and MENG B., Geochemistry and possible origin or crude oils from Bashituo Oilfield, Tarim Basin, (*in press; preliminary version published online Ahead of Print* 31 October 2018): AAPG Bulletin, doi:10.1306/10031817403.

STRASSER, A., and STROHMENGER, C., 1997, Early diagenesis in Pleistocene coral reefs, southern Sinai, Egypt: response to tectonics, sea−level and climate: Sedimentology, v. 44.3, p. 537-558.

SUN, S.Q., and ESTEBAN, M., 1994, Paleoclimatic controls on sedimentation, diagenesis, and reservoir quality: lessons from Miocene carbonates: AAPG bulletin, v. 78.4, p. 519-543.

TAGHAVI, A.A., MØRK, A., and EMADI, M.A., 2006, Sequence stratigraphically controlled diagenesis governs reservoir quality in the carbonate Dehluran Field, southwest Iran: Petroleum Geoscience, v. 12.2, p. 115-126.

TAN, K., MU, Z., LV, X., et al., 2004, The exploration potential of oil and gas of the carboniferous system in the Tarim southwest area: Natural Gas Geoscience, v. 15.12, p. 115-115 (Chinese, Abstract in English).

UENO, K., HAYAKAWA, N., NAKAZAWA, T., et al., 2013, Pennsylvanian–Early Permian cyclothemic succession on the Yangtze Carbonate Platform, South China: Geological Society, London, Special Publications, v. 376.1, p. 235-267.

VEIZER, J., ALA, D., and AZMY, K., et al., 1999, $^{87}Sr/^{86}Sr$, $\delta^{13}C$ and $\delta^{18}O$ evolution of Phanerozoic seawater: Chemical geology, v. 161.1, p. 59-88.

WANG, B., and Al-AASM, I.S., 2002, Karst-controlled diagenesis and reservoir development: Example from the Ordovician main-reservoir carbonate rocks on the eastern margin of the Ordos basin, China: AAPG bulletin, v. 86.9, p. 1639-1658.

WANG, X., FENG, Y., and CAO, Z., 2015, Application of various aspects of fluid inclusions in hydrocarbon formation history, taking Bachu-Maigaiti area of Tarim Basin as an example: Journal of Northeast Petroleum University, v. 39.2, p. 26-33(Chinese, Abstract in English).

XIAO, C., LI, L., JIANG, Y., et al., 1995, The Discovery Of Sedimentary Hiatus In Xiaohaizi Formation In Xiaohaizi Area, Bachu, Xinjiang And Its Geological Significance: Petroleum Exploration and Development, v. 22.3, p. 54-57 (Chinese, Abstract in English).

XIAO, C., and PAN, Y., 1999, Carboniferous Mixed Terrigenous Clastic, Carbonate and Sulphate Sediments in the Bachu Area, Xinjiang: Acta Geologica Sinica (English Edition), v. 73.3, p. 341-347.

YANG, S., YU, X., CHEN, H., et al., 2007, Geochemical characteristics and petrogenesis of Permian Xiaohaizi ultrabasic dyke in Bachu area, Tarim basin: Acta Petrologica Sinica, v. 23.5, p. 1087-1096 (Chinese, Abstract in English).

ZHANG, R., FENG, Q., ZHANG, H., et al., 2009, Characteristics and Control Factors of Carboniferous Bioclast Limestone Member Reservoir in the Qunkuqiake Area, Tarim Basin: ACTA GEOLOGICA SINICA, v. 83.4, p. 590-598 (Chinese, Abstract in English).

ZHANG, S., ZHANG, B., LI, B., et al., 2011a, History of hydrocarbon accumulations spanning important tectonic phases in marine sedimentary basins of China: Taking the Tarim Basin as an example: Petroleum Exploration and Development, v. 38.1, p. 1-15.

ZHANG, Z., LIU, S., YANG, Z., et al., 2011b, Tectonic evolution and its petroleum geological significances of the Maigaiti Slop, Tarim Basin: Oil&Gas Geology, v. 32.6, p. 909-919 (Chinese, Abstract in English).

ZHU, R., LUO, P., and LUO, Z., 2002, Lithofacies palaeogeography of the late Devonian and carboniferous in Tarim basin: Journal of Palaeogeography, v. 4.1, p. 13-24 (Chinese, Abstract in English).

ZHU, G., ZHANG, S., SU, J., et al., 2013, Secondary accumulation of hydrocarbons in Carboniferous reservoirs in the northern Tarim Basin, China: Journal of Petroleum Science and Engineering, v. 102, p. 10-26.

FIGURES CAPTIONS

Fig.1 (a). Location of the Bachu-Makit area in the western Tarim Basin; **(b)**. The distribut on of oil and gas field in the Bachu-Makit area; **(c).** The stratigraphic column of Carboniferous in the Bachu-Makit area.

Fig.2 Stratigraphic column and sedimentary environments of the Upper Carboniferous Xiaohaizi Formation in well BT4.

Fig.3 Lithology of the Xiaohaizi Formation. **(a).** Intrasparite limestone containing ooids, intraclast, and bioclast under plane-polarized light. The dark colours of grains were related to organic matters. The two generations of calcite cementation obstruct nearly all visible pores. **(b).**The image of (a) under cathode luminescence (CL). Note the CL colours of two generations of calcite cements are different. The early bladed calcites are non-luminescent, while the late blocky spars are dull orange. **(c)**.Fine crystalline intraclastic dolostone, cemented by poikilotopic calcite, under plane-polarized light. The crystals of dolomite are dull yellow. **(d)**.The image of (c) under CL. The CL colours of complete dolomitized grains are subtle null, while the poikilotopic calcites have dark orange colours. **(e)**. Intrasparite limestone with two phases of micro-fractures, under plane-polarized light. **(f)**. the image of (e) under CL. The CL colours of early micro-fractures are bright orange, while that of the late fracture are dark orange.

Fig.4 The features of subaerial exposure. **(a).** Vadose silt filled in the moldic pores of bioclast. VS-vadose silt. **(b).** Weathering breccia in intrasparite limestone, cemented by calcites. Br-breccia. **(c).** Several palaeosol layers on the brecciated dolostone in the

888 lower Xiaohaizi Formation, indicated by yellow arrows. **(d)**. SEM image of clay
889 minerals among dolomites.
890 **Fig.5** The features of dolomitization in the Xiaohaizi Formation. **(a)**.Dolomitic
891 intrasparite limestone with partly dolomitized grains, under plane-polarized light. The
892 crystals of dolomite inside grains are dirty and fine. The two generations of calcite
893 cements obstructed nearly all visible pores. Cc-calcite; Cc-I-the first generation of
894 calcite; Cc-II-the second generation of calcite; **(b)**. The image of (a) under cathode
895 luminescence (CL). Partially dolomitized grains have dark red colours under CL,
896 minor dark orange. The CL colours of early bladed calcites are dull, caused by very
897 low Mn^{2+}. The late blocky calcites have dark orange colours under CL, indicating a
898 low Mn^{2+} or high Fe^{2+} diagenetic environment. **(c).** Dolomitic intramicrite, under
899 plane-polarized light. The grains have partly dolomitized, while the matrix is
900 completely dolomitized. The bladed calcites grow around grains as isopachous fringes.
901 **(d).** The image of (c) under CL. The partly dolomitized grains have weak orange
902 colours. The colours of bladed calcite are null, while the micritic dolomites have weak
903 red colours. **(e)**. Intraclastic dolostone, under plane-polarized light. The dolomitized
904 grains are dark earthy yellow. Poikilotopic calcites and fluorites fill in the pores. **(f).**
905 The image of (e) under CL. The colours of complete dolomitized grains are subtle dull,
906 indicating a very low Mn^{2+} environment. Poikilotopic calcites have dark to bright
907 orange colours. The fluorites have deep blue colours. **(g)**. The SEM image of
908 dolomitized grains, with the crystal size ranging from14-32μm. **(h).** The SEM image

909 of organic matters among dolomites. These organic matter contain abundant C, N, O,
910 belonging to the component of palaeosol. OM-organic matter.

911 **Fig.6** The photos of diagenetic minerals in the Xiaohaizi Formation. **(a).** The SEM
912 image of dickites. The blocky dickite crystals, with size of 3-13μm, have the spatial
913 organization seems inherited from pre-existing booklets. **(b).** The image of kaolinites
914 filling in intergranular dissolved pores among dolomitized grains, under
915 plane-polarized light. Blue areas are pores. **(c).** Dickites fill within intergranular
916 dissolved pores, under cross-polarized light. Dickites have interference colour of
917 greyish white. **(d).** The image of (c) under cathode luminescence (CL). Dickites have
918 deep blue colours under CL. The dissolved dolomites were enclosed by dickites. **(e).**
919 Euhedral crystal of fluorite grows in dolostone. Opaque pyrites are oserved. **(f).** The
920 image of (e) under CL. The colour of fluorite is bluish-violet. **(g).** The image of
921 fluorites and dickites under CL, from Fu et al., 2012b. The dickites were enclosed in
922 fluorites, indicating precipitation of fluorites postdated dickites. **(h).** The SEM image
923 of pyrite on thin section. Authigenic pyrite filled in the dissolved pores, postdating
924 dissolution. **(i).** The image of overgrowth quartz under cross-polarized light. The
925 overgrowth quartz grows towards intergranular pores. It shows quartz overgrowth
926 occurred after compaction. There are fine crystals of dolomite existing between
927 detrital quartz and overgrowth quartz. **(j).** The image of anhydrite in the partly
928 dolomitized intrasparite under cross-polarized light. The bright interference colour
929 and plate like structure can be identified as anhydrite.

930 **Fig.7** The vertical variation of content of terrigenous quartz, carbon and oxygen
931 isotope of the Xiaohaizi Formation in well M10. Note that there are two cycles of
932 inter-glaciation period and glaciation period. The high content of quartz and
933 enrichment of ^{18}O stands for the onset of glacial period.

934 **Fig.8** The photos of different types of pores in the Xiaohaizi Foramtion. **(a).** The
935 image of intragranular pore under plane-polarized light. **(b).** The non-fabric selective
936 pores filled with calcite, under plane-polarized light. **(c).** The image of dissolved
937 intergranular pores, under plane-polarized light. Paritally dissolved feldspar (yellow
938 arrow) is present. **(d).** The image of primary intergranular pores in intrasparite, under
939 plane-polarized light. DIP: dissolved intergranular pore; IP: intergranular pore; IAP:
940 intragranular pore; Cc: calcite; Do: dolomite.

941 **Fig.9** The cross plots of porosity and permeability. (a).The bulk data for all samples.
942 There is a good positive correlation, with coefficient of 0.7677. **(b).** The relationship
943 between lithology and physical property. The dolostones have highest porosity and
944 permeability than other rocks.

945 **Fig.10** The correlation analysis of physical property, lithology and rock components.
946 **(a).** The cross plot of terrigenous grains contents and biodetritus contents within
947 whole rock; **(b).** The porosities of reservoir rocks from different microfacies of
948 carbonate shoals; **(c).** The cross plot of porosities of reservoir rocks and contents of
949 detrial quartz within whole rock; **(d).** The cross plot of porosities of reservoir rocks
950 and contents of dolomite within whole rock.

951 **Fig.11** Paragenesis of the carbonate rocks from the Xiaohaizi Formation.

952 **Fig.12** The transformation pathway of kaolinite and dickite in the Xiaohaizi
953 Formation.

954 **Fig.13** The homogeneous temperatures of fluid inclusions within the calcite veins of
955 the Xihaozi Formation in well BT4.

956 **Fig.14** The depositional and diagenetic model of the Xiaohaizi Formation during the
957 cycle of interglaciation and glaciation. The mixed siliciclastic-carbonate
958 sedimentation and subaerial exposure controls the formation of porous dolostones, as
959 response to the sea level fall with proceeding of glaciation. Dolostones with weak
960 cementation have abundant pores to be the best reservoir rocks.

Table 1 The information of drilling cores from the Xiaohaizi Formation in six wells

Well	Length of cores (m)	Top depth (m)	Bottom depth (m)
BT4	18.92	4301	4319.92
BT8	52.17	4483.53	4535.7
M10	37.42	4394	4431.42
BT3	15.89	1911.42	1927.31
BT6	16.12	4438.6	4454.72
M4	5.4	4385.5	4390.9

Table 2 The content of components in part of carbonate rocks from the Xiaohaizi Formation

Well	Depth (m)	Lithology	Content of component (vol. %)							Assembly of creatures
			intraclastic	bioclastic	oncoid	ooid	terrigeous detrital grain	micrite matrix	cement	
BT4	4301.64	Oosparite limestone	25	10	5	35	/	/	25	echinodermata, bryozoan,brachiopod
BT4	4302.16	Biosparite limestone	10	56	/	/	4	/	30	green algae,fusulinid, echinodermata, brachiopod
BT4	4302.87	Biosparite limestone	8	59	/	/	8	/	25	fusulinid, echinodermata, brachiopod
BT4	4308.63	Intrasparite limestone	45	25	/	/	/	/	30	fusulinid, echinodermata, brachiopod
BT4	4304	Biosparite limestone	5	60	/	/	10	/	25	foraminifera, echinodermata, brachiopod
BT4	4315.24	Intrasparrudite limestone	55	20	/	/	/	/	25	fusulinid, echinodermata, brachiopod
BT8	4483.03	Biomicrite	/	65	/	/	/	35	/	foraminifera, echinodermata, brachiopod
BT8	4484.12	Biosparite limestone	30	40	10	/	/	/	20	echinodermata,green algae,brachiopod, foraminifera,bryozoan,gastropods
BT8	4493.24	Partly dolomitized oosparite limestone	15	5	/	51	1	/	28	brachiopod,bivalve, echinodermata
BT8	4495.95	Partly dolomitized intrasparite limestone	71	4	/	/	/	/	25	echinodermata,brachiopod,green algae,fusulinid

Table 3 The composition of minerals determined by XRD from the Xiaohaizi Formation

Well	Depth（m）	Lithology	Content of minerals (wt.%)					
			Kaolinite	Quartz	Calcite	Dolomite	Pyrite	Anhydrite
M10	4397.30	dolostone	/	1	3	96	/	
M10	4398.10	calcareous dolostone	2	2	33	63	/	
M10	4400.10	calcareous dolostone	1	2	27	70	/	
M10	4406.54	calcareous dolostone	/	/	25	75	/	
M10	4404.94	calcareous dolostone	/	/	21	79	/	
BT4	4312.11	dolostone	6	/	9	84	1	
BT3	1918.02	dolostone	/	1	2	97	/	
BT3	1921.48	calcareous dolostone	1	1	48	50	/	
BT3	1924.11	limestone	1	3	95	1	/	
BT3	1924.11	limestone	1	3	96	/	/	

/: none

Table 4 The composition of terrigenous elements in carbonate rocks from the Xiaohaizi Formation

Well	Depth(m)	Position of sample	Concentration of elements (μg/g)						
			Al	Sr	Ba	Ti	Cr	Rb	K
BT3	1924.11	adjacent to palaeosol	9619.01	463.49	243.01	225.67	9.17	8.89	2171.52
	1924.11		9415.54	509.80	665.88	236.82	10.47	10.11	1907.77
	1924.11		7262.50	384.00	233.50	251.00	18.50	25.62	2300.25
BT3	1918.02	undersea	4993.07	118.88	11.15	48.79	5.94	1.62	351.69
BT4	4306.93		6792.48	207.07	16.62	99.20	30.01	2.36	586.50
BT4	4312.11		6555.00	174.50	44.50	193.75	23.25	3.69	643.00
BT4	4316.09		3698.15	268.37	178.41	37.73	7.75	0.96	327.09
BT4	4217.55		3880.00	220.50	6.25	46.50	22.50	\	535.25
M10	4397.30		4480.00	673.50	11.75	95.00	12.00	3.27	494.75
M10	4398.10		6016.59	166.37	20.11	120.43	27.81	1.45	640.40
M10	4400.10		5260.00	176.25	8.50	107.00	26.75	2.06	344.75
M10	4404.94		3400.00	167.25	3.00	45.75	10.25	1.04	152.25
M10	4406.54		5315.00	158.50	29.25	47.75	10.00	1.66	354.00

Table 5 Summary chart of the petrologic characteristic in different depositional environments

Depositional facies			Lithology	Color	Structure	Texture	Physical property	Porosity(%)
Facies	Sub-facies	Mirco-facies						
mixed siliciclastic-carbonate platform	lagoon	Marl	Marly limestone	Dark grey	Fracture	Matrix-supported	Extreme Poor	none
	Carbonate shoal	Bioclastic shoal	Biosparite limestone, biogenic dolostones, partly dolomitized biosparite limestone	White	Stylolite, vug	Grain-supported	Very Poor-Very good	0.8-13.5
		Oolitic shoal	Oosparite limestone，	White	Fracture, stylolite	Grain-supported	Very Poor	1.2-2.0
		Intraclastic shoal	Partly dolomitized intrasparite limestone, finely crystalline intraclastic dolostones	Yellow grey, dark earthy yellow	Fracture, vug	Grain-supported, residual grain fabric	Very Poor-Very good	0.4-16.6
		Subtidal zone	Dolomicrite	Grey	Laminar algal	Microcrystalline	Very Poor-Poor	0.8-7.4

Table 6 Summary chart of the main diagenesis and their effect on reservoir quality

Type of main diagenesis	Diagenetic mineral	Diagentic environment	Supporting evidence	Effect on reservoir quality
Early calcite cementation	Bladed calcite, blocky calcite,	Sea water	Dull and weak organce CL color	Destructive
Dissolution by meteoric water	Blocky calcite, kaolinte	Subaerial exposure	Vadose silt, palaeosol	Constructive
Dissolution and cementation related to hydrothermal fluid	Fluorite, pyrite, dickite, poikilitic calcite	Hydrothermal fluid	Assembly of fluorite, pyrite, and dickite; High TH ，high concentration of Mn^{2+}	Constructive /destructive
Dolomitization	Dolomite	Low-temperature, episodical restricted environment; Shallow buried	Small, euhedral and cloudy crystals, dull to dark red CL color	Constructive
Quartz overgrowth	Overgrowth quartz	Moderate to deep buried	Euhedral crystal	Irrelevant/destructive

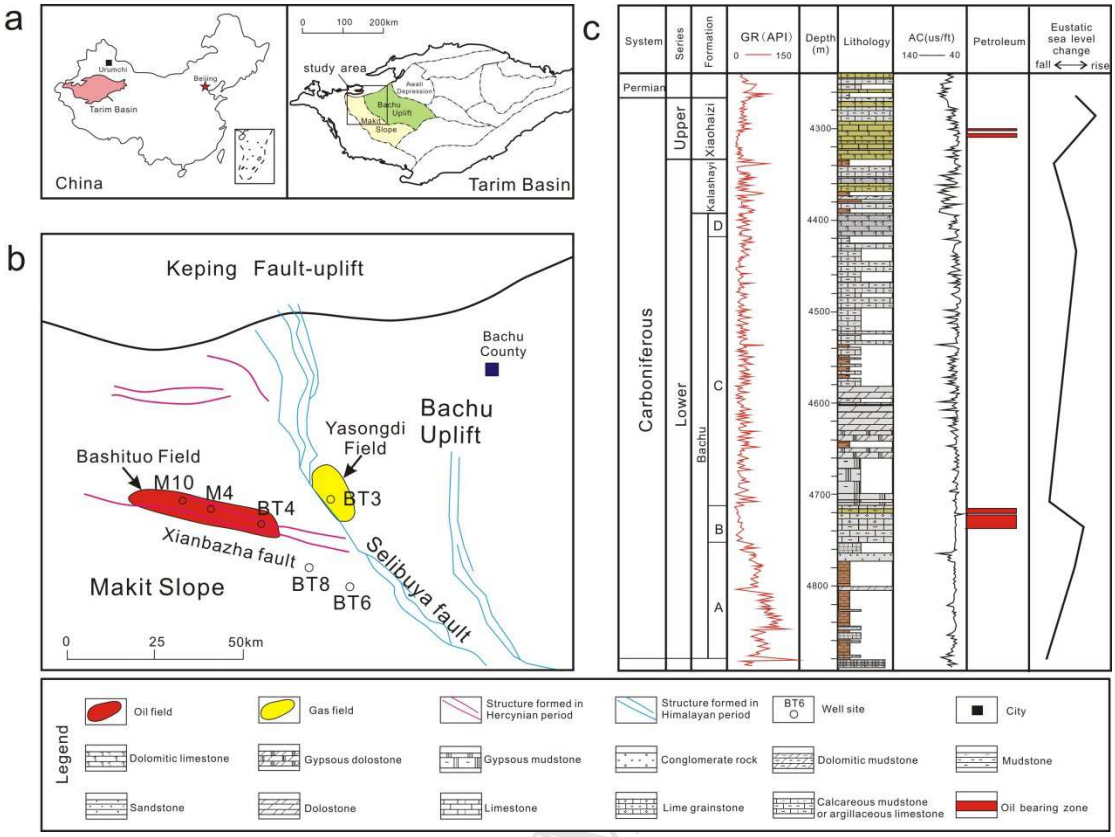

Fig.1 (a). Location of the Bachu-Makit area in the western Tarim Basin; **(b).** The distribut on of oil and gas field in the Bachu-Makit area; **(c).** The stratigraphic column of Carboniferous in the Bachu-Makit area.

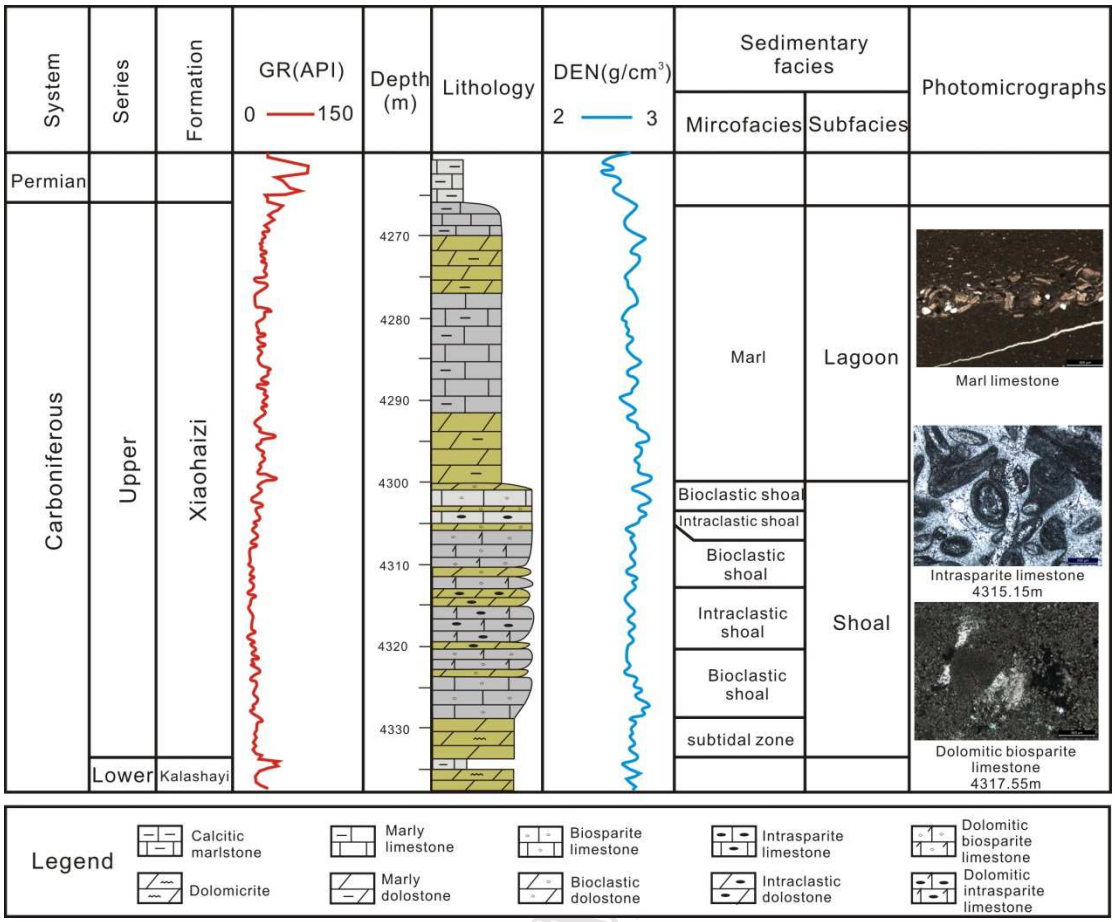

Fig.2 Stratigraphic column and sedimentary facies of the Upper Carboniferous Xiaohaizi Formation in well BT4.

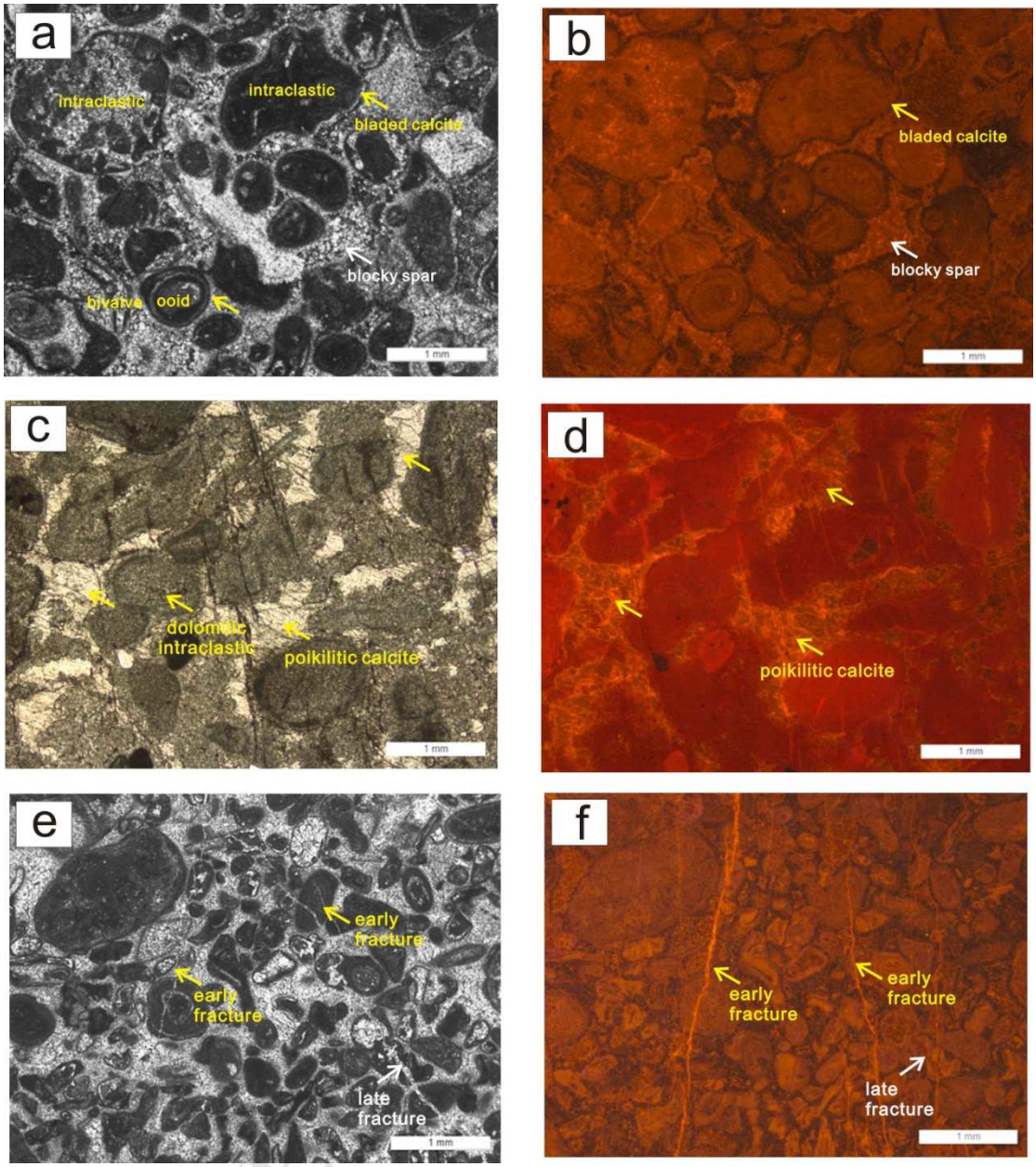

Fig.3 Lithology of the Xiaohaizi Formation **(a).** Intrasparite limestone containing ooids, intraclast, and bioclast under plane-polarized light. The dark colours of grains were related to organic matters. The two generations of calcite cementation obstruct nearly all visible pores. **(b).**The image of (a) under cathode luminescence (CL). Note the CL colours of two generations of calcite cements are different. The early bladed calcites are non-luminescent, while the late blocky spars are dull orange. **(c)**.Fine crystalline intraclastic dolostone, cemented by poikilotopic calcite, under plane-polarized light. The crystals of dolomite are dull yellow. **(d)**.The image of (c) under CL. The CL colours of complete dolomitized grains are subtle null, while the poikilotopic calcites have dark orange colours. **(e)**. Intrasparite limestone with two phases of micro-fractures, under plane-polarized light. **(f)**. the image of (e) under CL. The CL colours of early micro-fractures are bright orange, while that of the late fracture are dark orange.

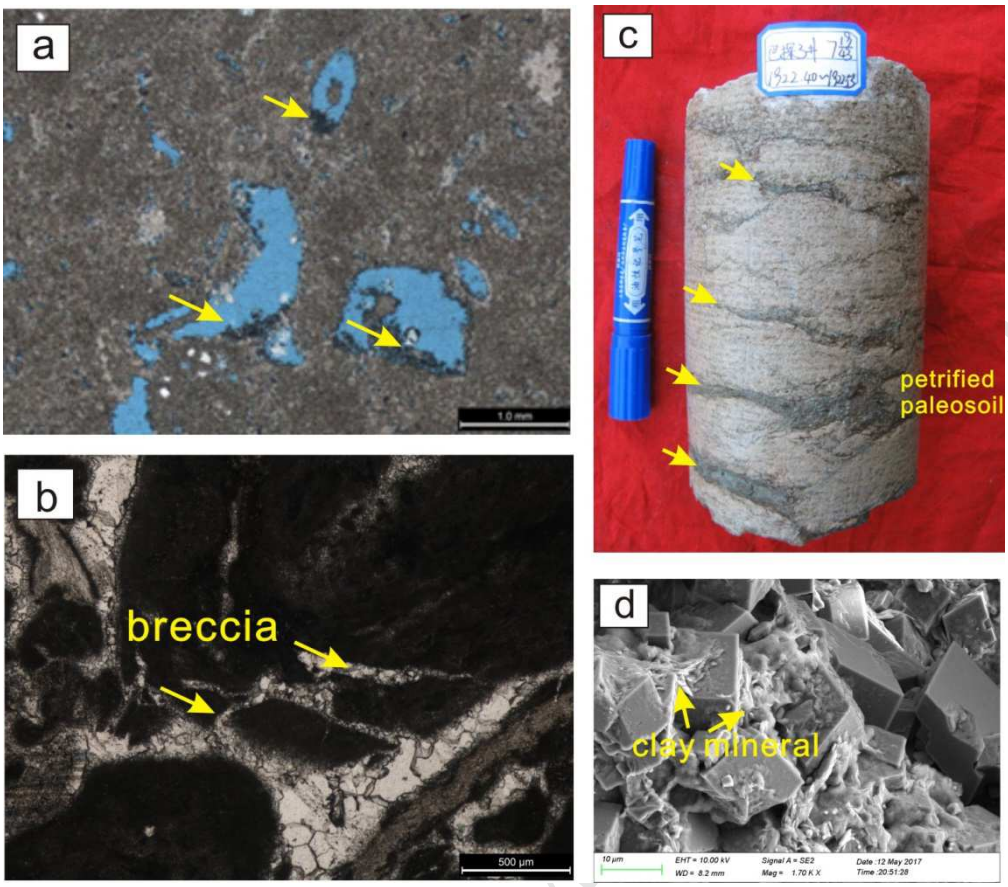

Fig.4 The features of subaerial exposure. **(a).** Vadose silt filled in the moldic pores of bioclast. VS-vadose silt. **(b).** Weathering breccia in intrasparite limestone, cemented by calcites. Br-breccia. **(c).** Several palaeosol layers on the brecciated dolostone in the lower Xiaohaizi Formation, indicated by yellow arrows. **(d)**. SEM image of clay minerals among dolomites.

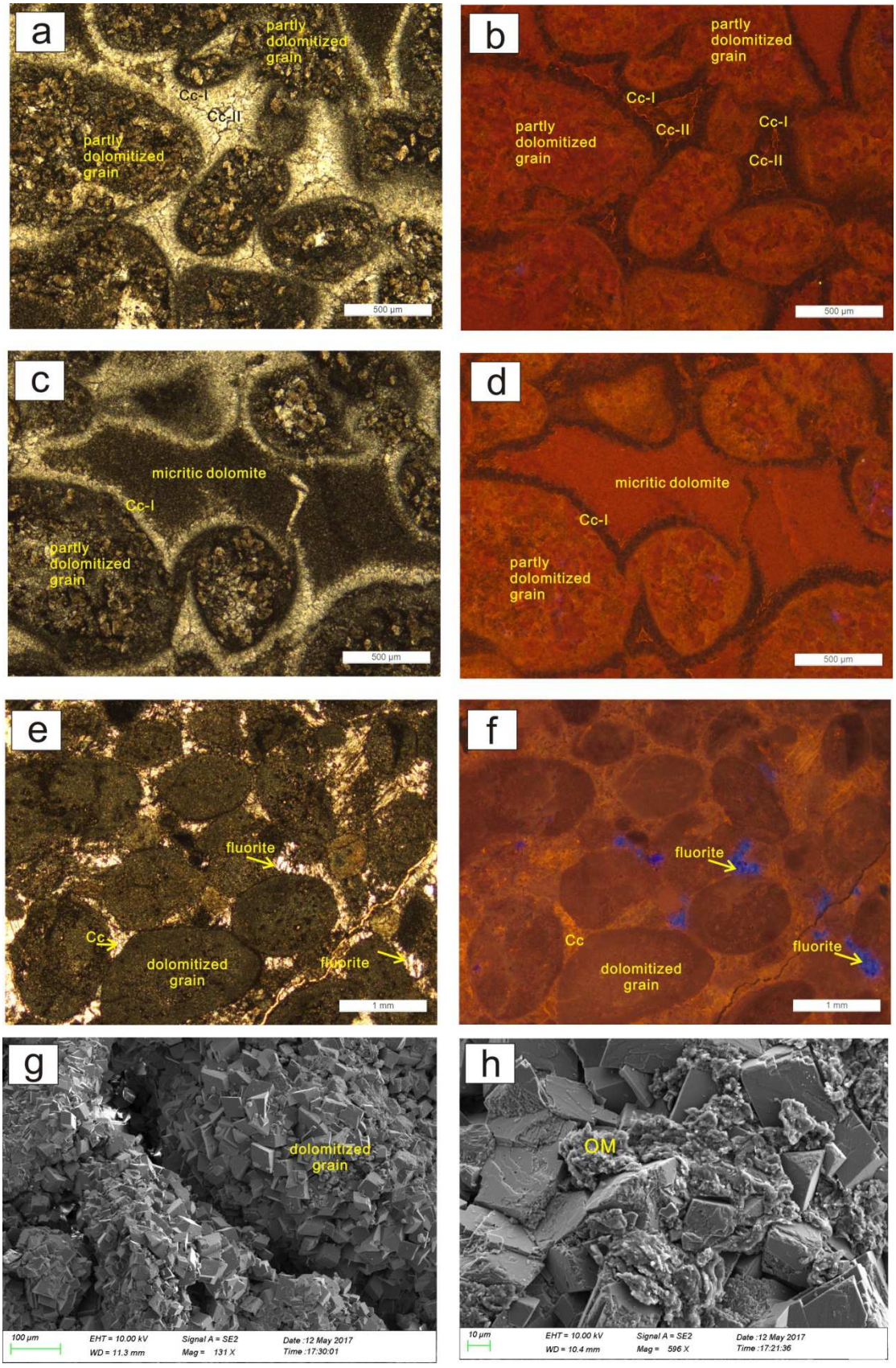

Fig.5 The features of dolomitization in the Xiaohaizi Formation. **(a)**.Dolomitic intrasparite limestone with partly dolomitized grains, under plane-polarized light. The

crystals of dolomite inside grains are dirty and fine. The two generations of calcite cements obstructed nearly all visible pores. Cc-calcite; Cc-I-the first generation of calcite; Cc-II-the second generation of calcite; **(b)**. The image of (a) under cathode luminescence (CL). Partially dolomitized grains have dark red colours under CL, minor dark orange. The CL colours of early bladed calcites are dull, caused by very low Mn^{2+}. The late blocky calcites have dark orange colours under CL, indicating a low Mn^{2+} or high Fe^{2+} diagenetic environment. **(c).** Dolomitic intramicrite, under plane-polarized light. The grains have partly dolomitized, while the matrix is completely dolomitized. The bladed calcites grow around grains as isopachous fringes. **(d).** The image of (c) under CL. The partly dolomitized grains have weak orange colours. The colours of bladed calcite are null, while the micritic dolomites have weak red colours. **(e)**. Intraclastic dolostone, under plane-polarized light. The dolomitized grains are dark earthy yellow. Poikilotopic calcites and fluorites fill in the pores. **(f).** The image of (e) under CL. The colours of complete dolomitized grains are subtle dull, indicating a very low Mn^{2+} environment. Poikilotopic calcites have dark to bright orange colours. The fluorites have deep blue colours. **(g)**. The SEM image of dolomitized grains, with the crystal size ranging from14-32μm. **(h).** The SEM image of organic matters among dolomites. These organic matter contain abundant C, N, O, belonging to the component of palaeosol. OM-organic matter.

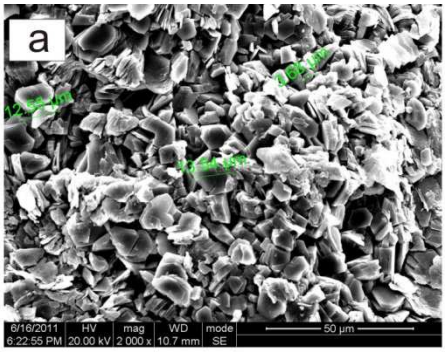
a
6/16/2011 6:22:55 PM
HV 20.00 kV
mag 2 000 x
WD 10.7 mm
mode SE
50 µm

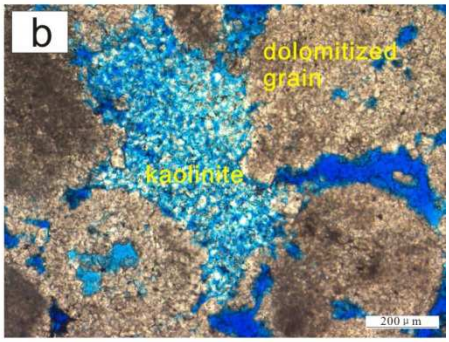
b
dolomitized grain
kaolinite
200 µ m

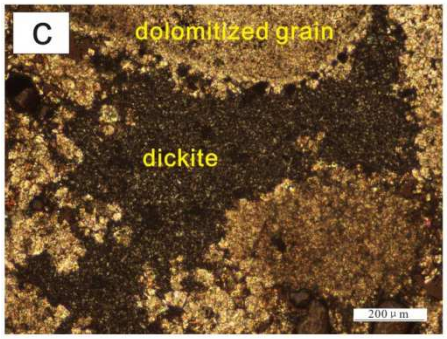
c
dolomitized grain
dickite
200 µ m

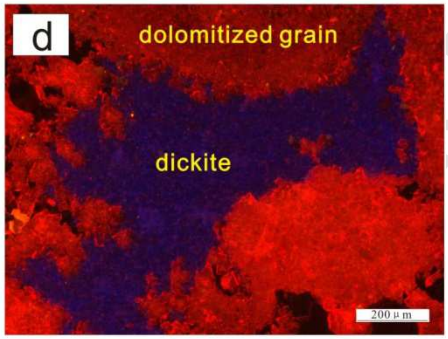
d
dolomitized grain
dickite
200 µ m

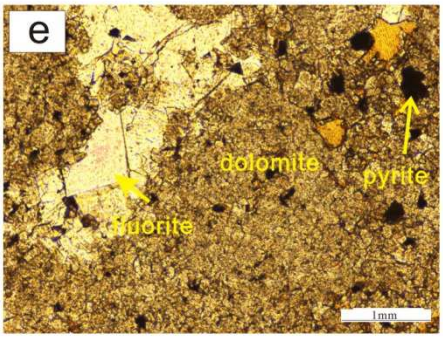
e
dolomite
pyrite
fluorite
1 mm

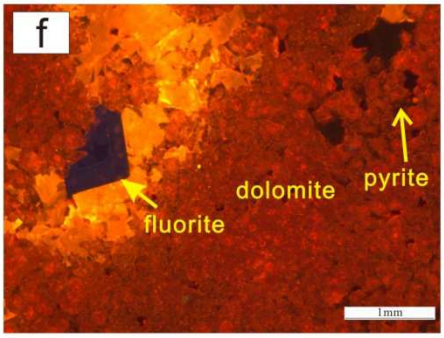
f
dolomite
pyrite
fluorite
1 mm

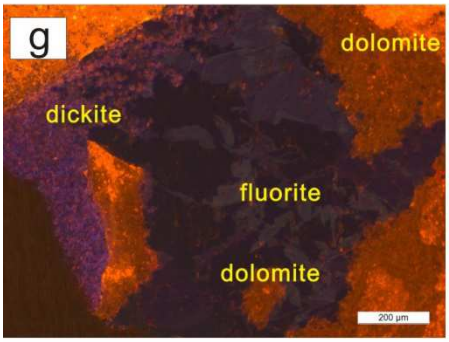
g
dolomite
dickite
fluorite
dolomite
200 µm

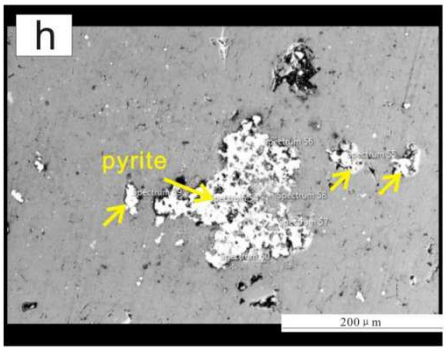
h
pyrite
200 µ m

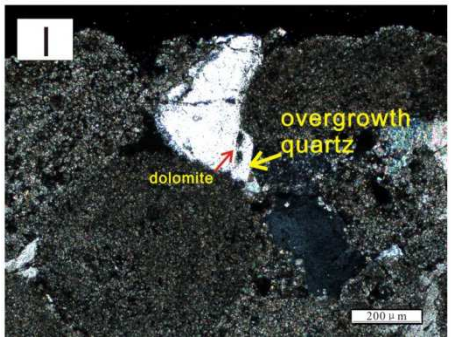
I
overgrowth quartz
dolomite
200 µ m

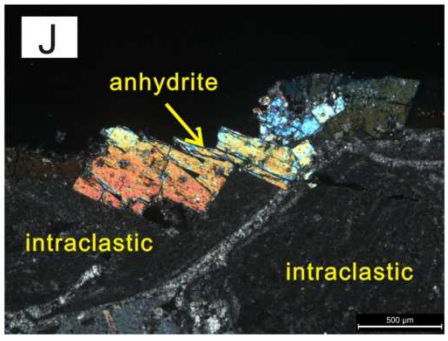
J
anhydrite
intraclastic
intraclastic
500 µm

Fig.6 The photos of diagenetic minerals in the Xiaohaizi Formation. **(a).** The SEM image of dickites. The blocky dickite crystals, with size of 3-13μm, have the spatial organization seems inherited from pre-existing booklets. **(b).** The image of kaolinites filling in intergranular dissolved pores among dolomitized grains, under plane-polarized light. Blue areas are pores. **(c).** Dickites fill within intergranular dissolved pores, under cross-polarized light. Dickites have interference colour of greyish white. **(d).** The image of (c) under cathode luminescence (CL). Dickites have deep blue colours under CL. The dissolved dolomites were enclosed by dickites. **(e).** Euhedral crystal of fluorite grows in dolostone. Opaque pyrites are oserved. **(f).** The image of (e) under CL. The colour of fluorite is bluish-violet. **(g).** The image of fluorites and dickites under CL, from Fu et al., 2012b. The dickites were enclosed in fluorites, indicating precipitation of fluorites postdated dickites. **(h).** The SEM image of pyrite on thin section. Authigenic pyrite filled in the dissolved pores, postdating dissolution. **(I).** The image of overgrowth quartz under cross-polarized light. The overgrowth quartz grows towards intergranular pores. It shows quartz overgrowth occurred after compaction. There are fine crystals of dolomite existing between detrital quartz and overgrowth quartz. **(J).** The image of anhydrite in the partly dolomitized intrasparite under cross-polarized light. The bright interference colour and plate like structure can be identified as anhydrite.

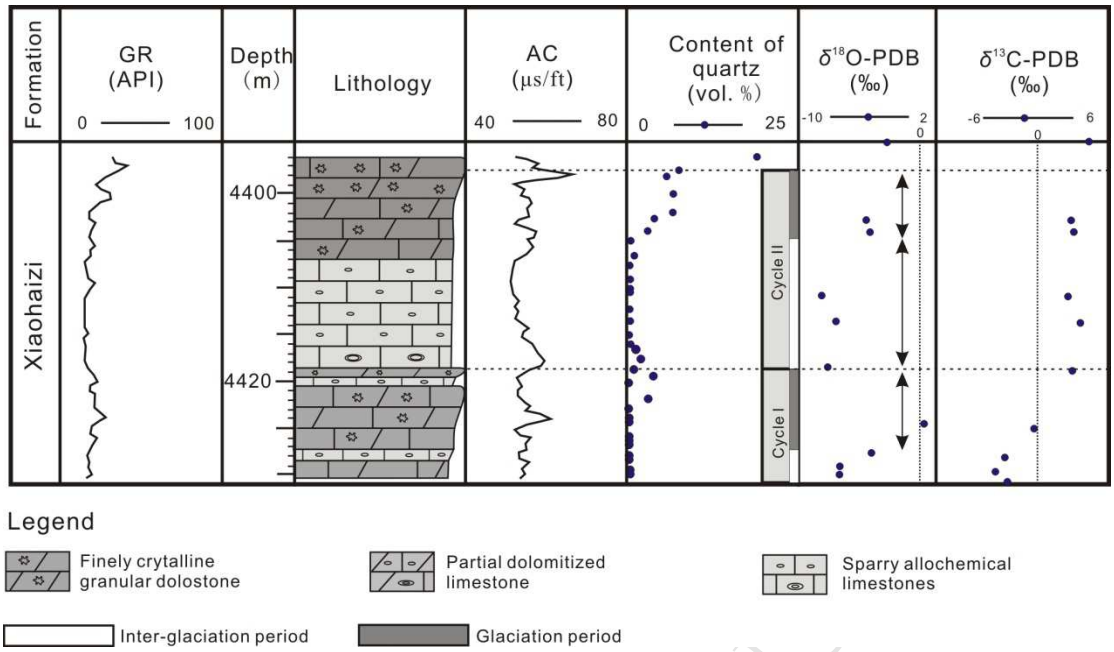

Fig.7 The vertical variation of content of terrigenous quartz, carbon and oxygen isotope of the Xiaohaizi Formation in well M10. Note that there are two cycles of inter-glaciation period and glaciation period. The high content of quartz and enrichment of ^{18}O stands for the onset of glacial period.

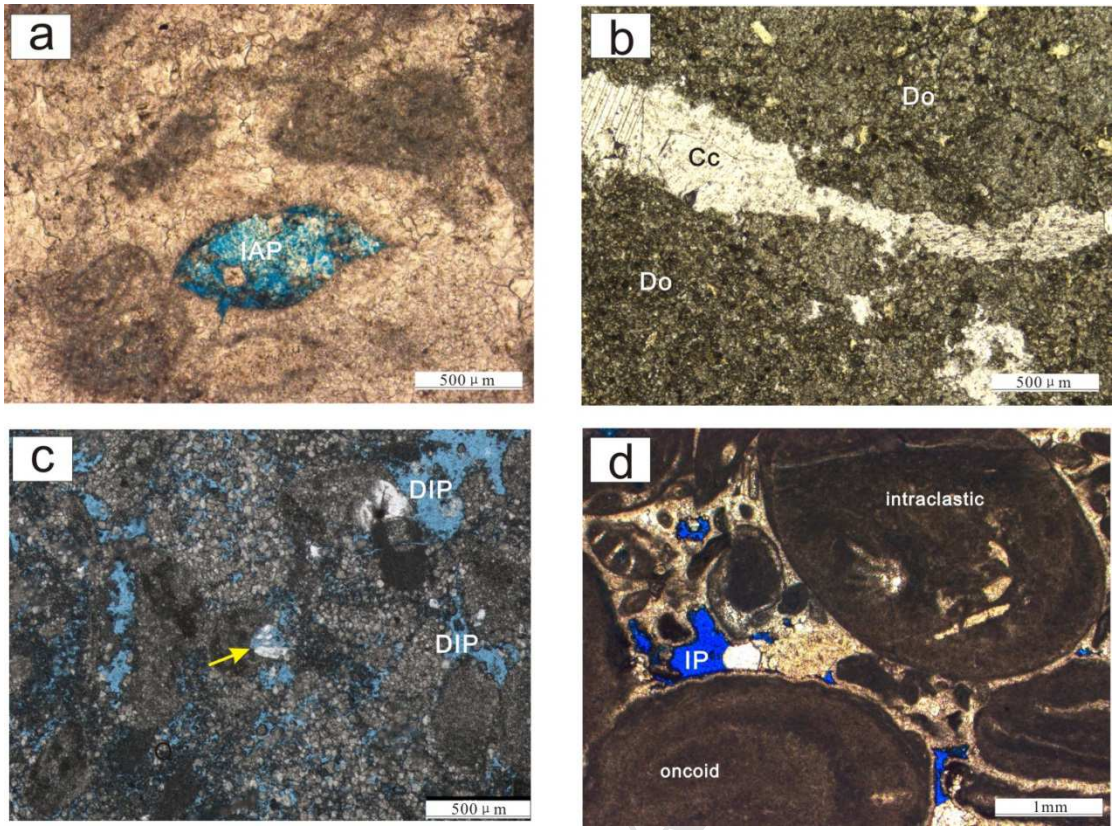

Fig.8 The photos of different types of pores in the Xiaohaizi Foramtion. **(a).** The image of intragranular pore under plane-polarized light. **(b).** The non-fabric selective pores filled with calcite, under plane-polarized light. **(c).** The image of dissolved intergranular pores, under plane-polarized light. Paritally dissolved feldspar (yellow arrow) is present. **(d).** The image of primary intergranular pores in intrasparite, under plane-polarized light. DIP: dissolved intergranular pore; IP: intergranular pore; IAP: intragranular pore; Cc: calcite; Do: dolomite.

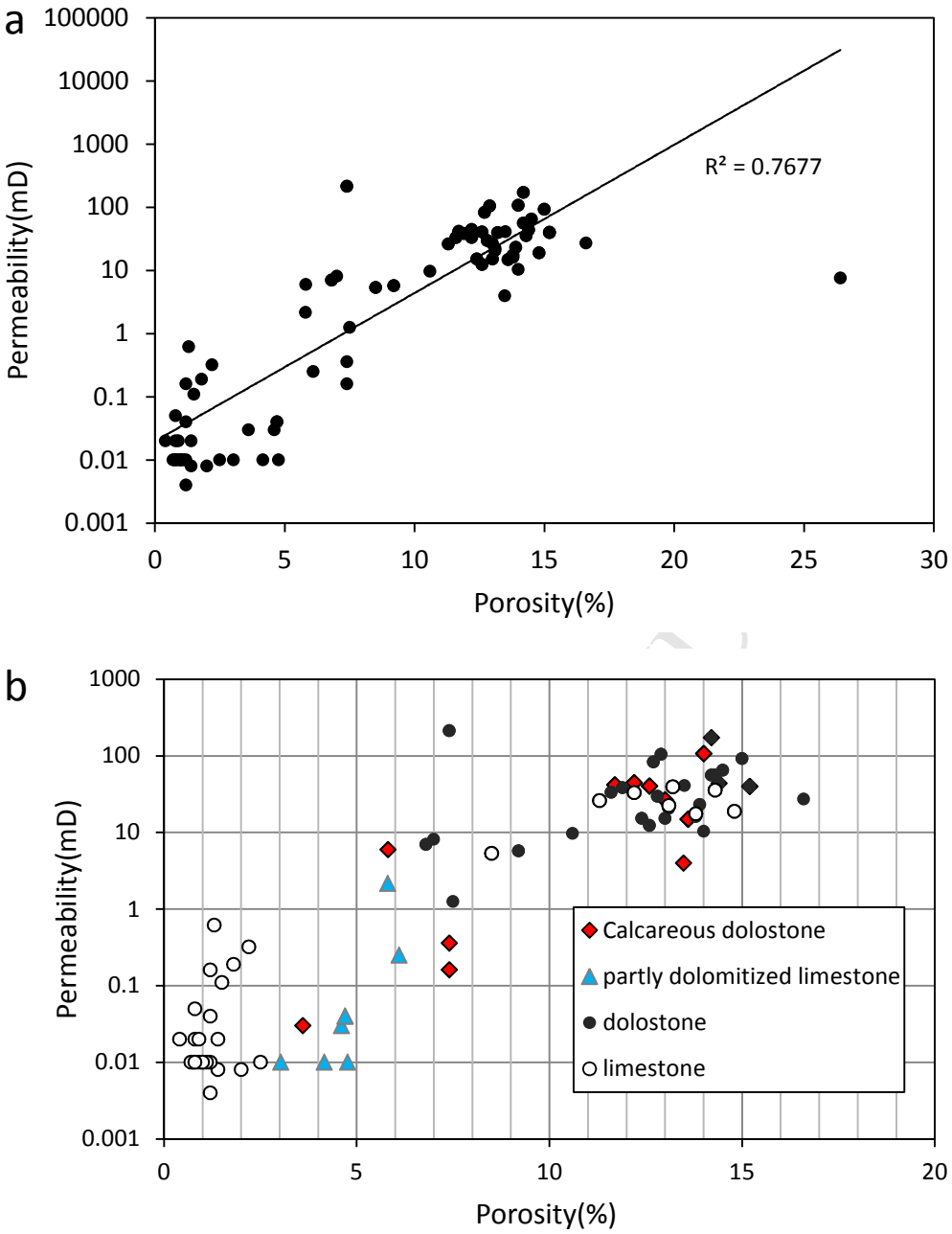

Fig.9 The cross plots of porosity and permeability. **(a).**The bulk data for all samples. There is a good positive correlation, with coefficient of 0.7677. **(b).** The relationship between lithology and physical property. The dolostones have highest porosity and permeability than other rocks.

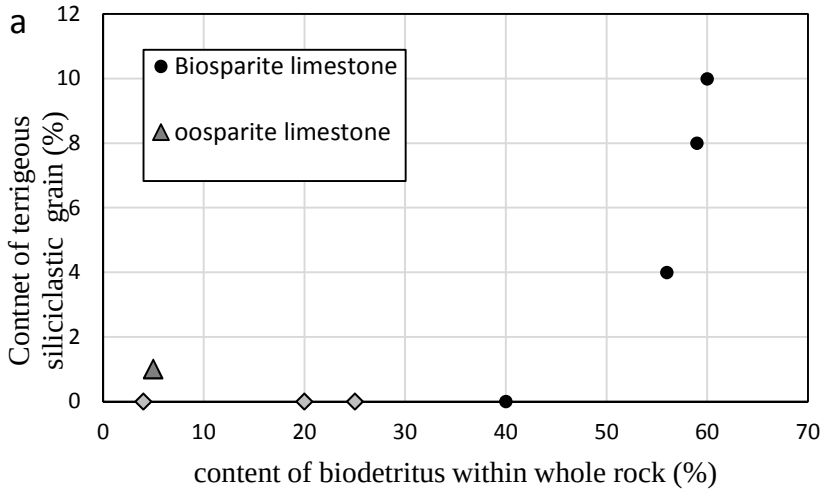
a
Biosparite limestone
oosparite limestone
Contnet of terrigeous siliciclastic grain (%)
content of biodetritus within whole rock (%)

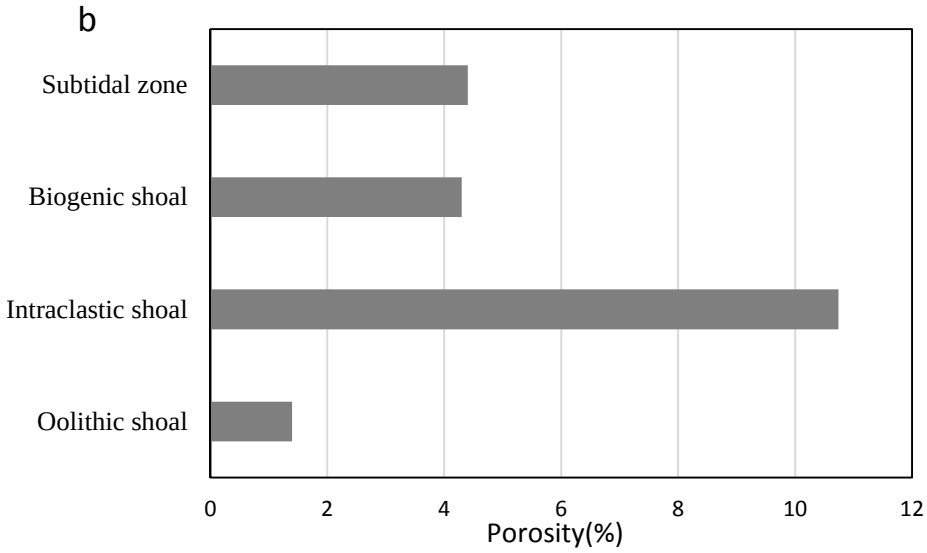
b
Subtidal zone
Biogenic shoal
Intraclastic shoal
Oolithic shoal
Porosity(%)

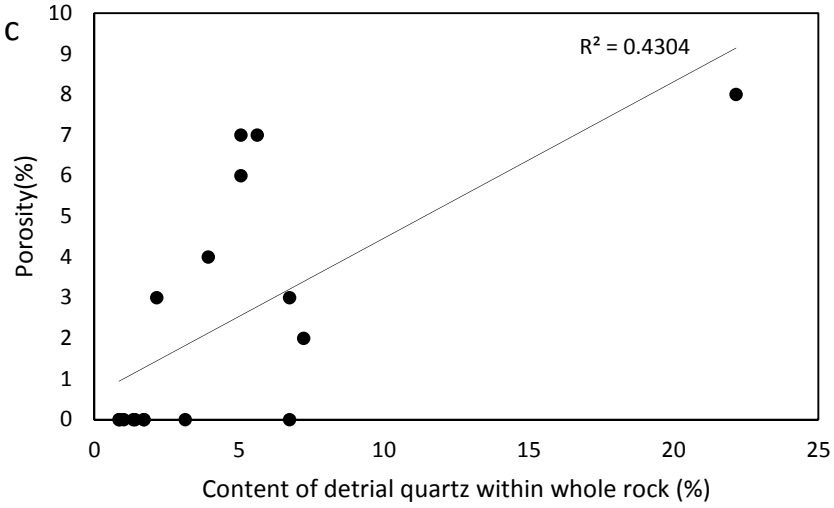
c
R² = 0.4304
Porosity(%)
Content of detrial quartz within whole rock (%)

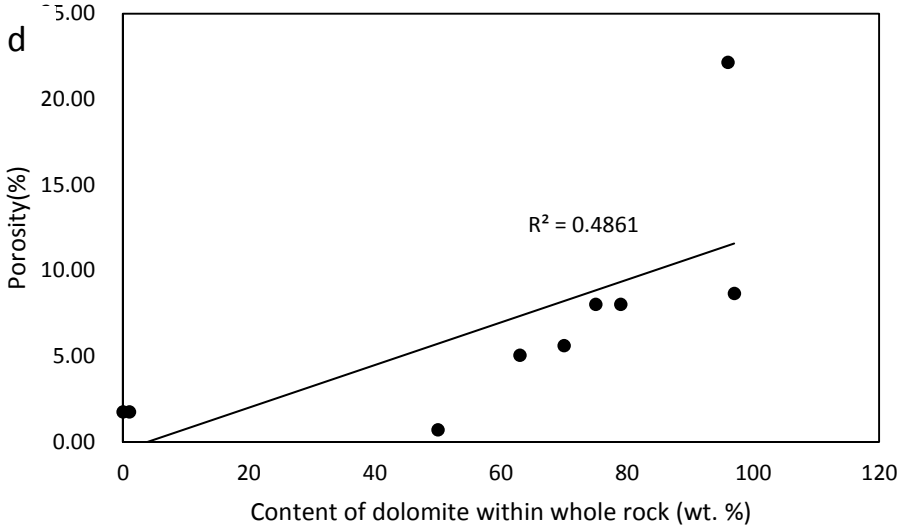

Fig.10 The correlation analysis of physical property, lithology and rock components. **(a).** The cross plot of terrigenous grains contents and biodetritus contents within whole rock; **(b).** The porosities of reservoir rocks from different microfacies of carbonate shoals; **(c).** The cross plot of porosities of reservoir rocks and contents of detrial quartz within whole rock; **(d).** The cross plot of porosities of reservoir rocks and contents of dolomite within whole rock.

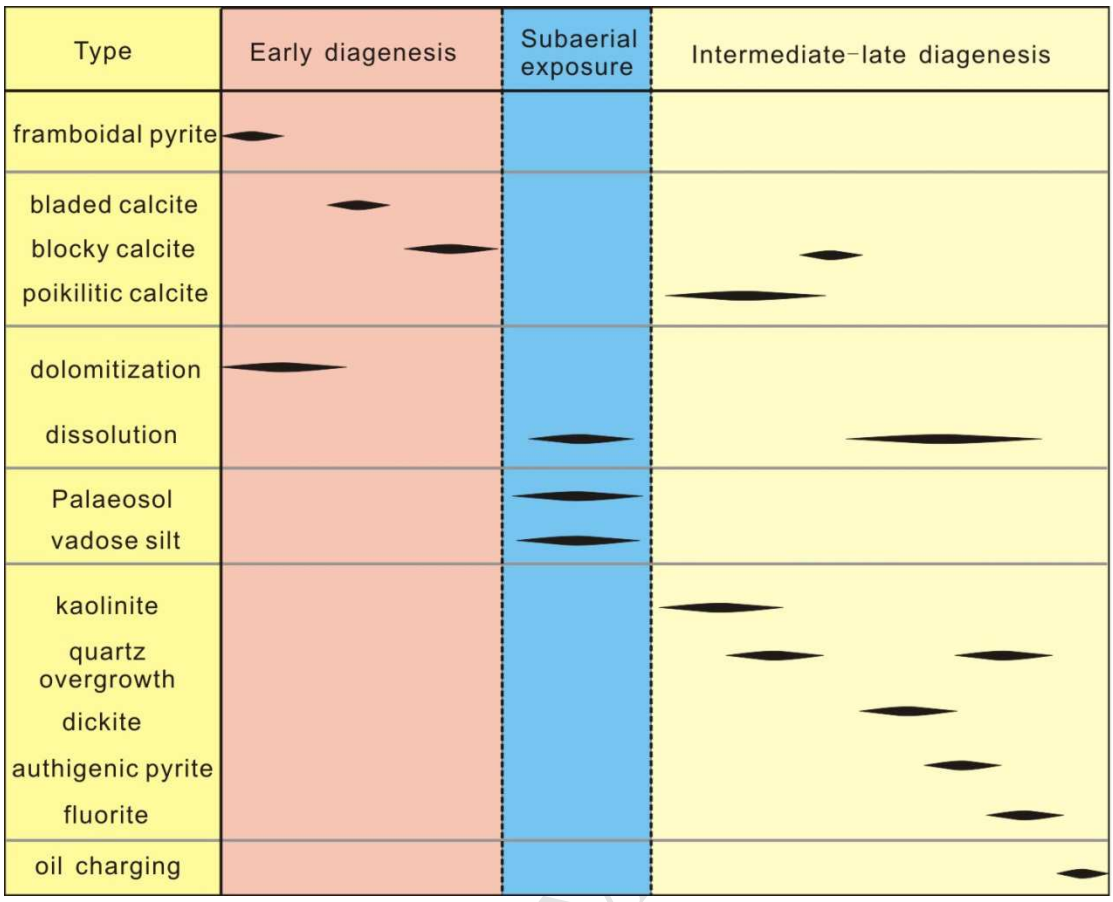

Fig.11 Paragenesis of the carbonate rocks from the Xiaohaizi Formation

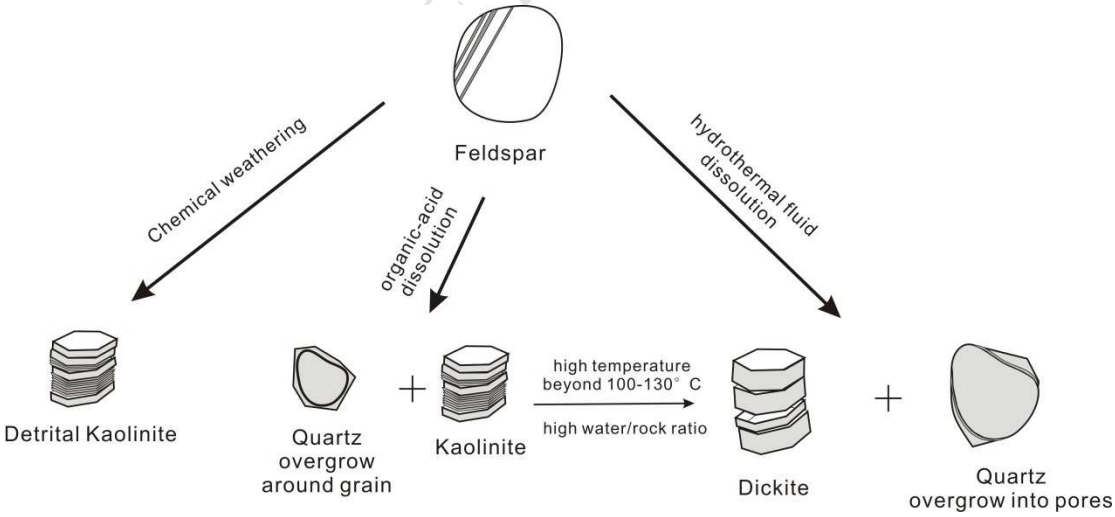

Fig.12 The transformation pathway of kaolinite and dickite in the Xiaohaizi Formation

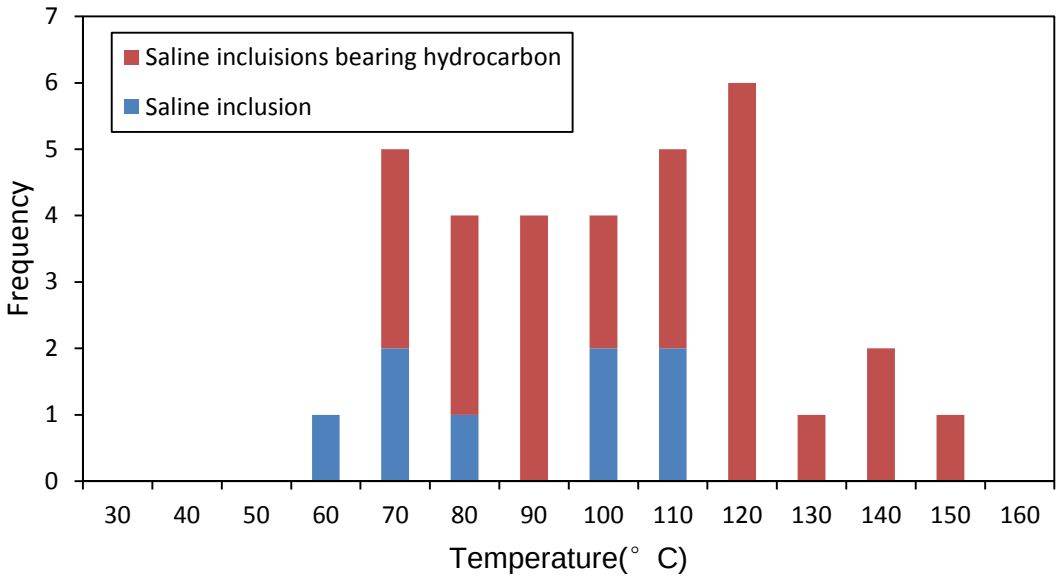

Fig.13 The homogeneous temperatures of fluid inclusions within the calcite veins of the Xihaozi Formation in well BT4.

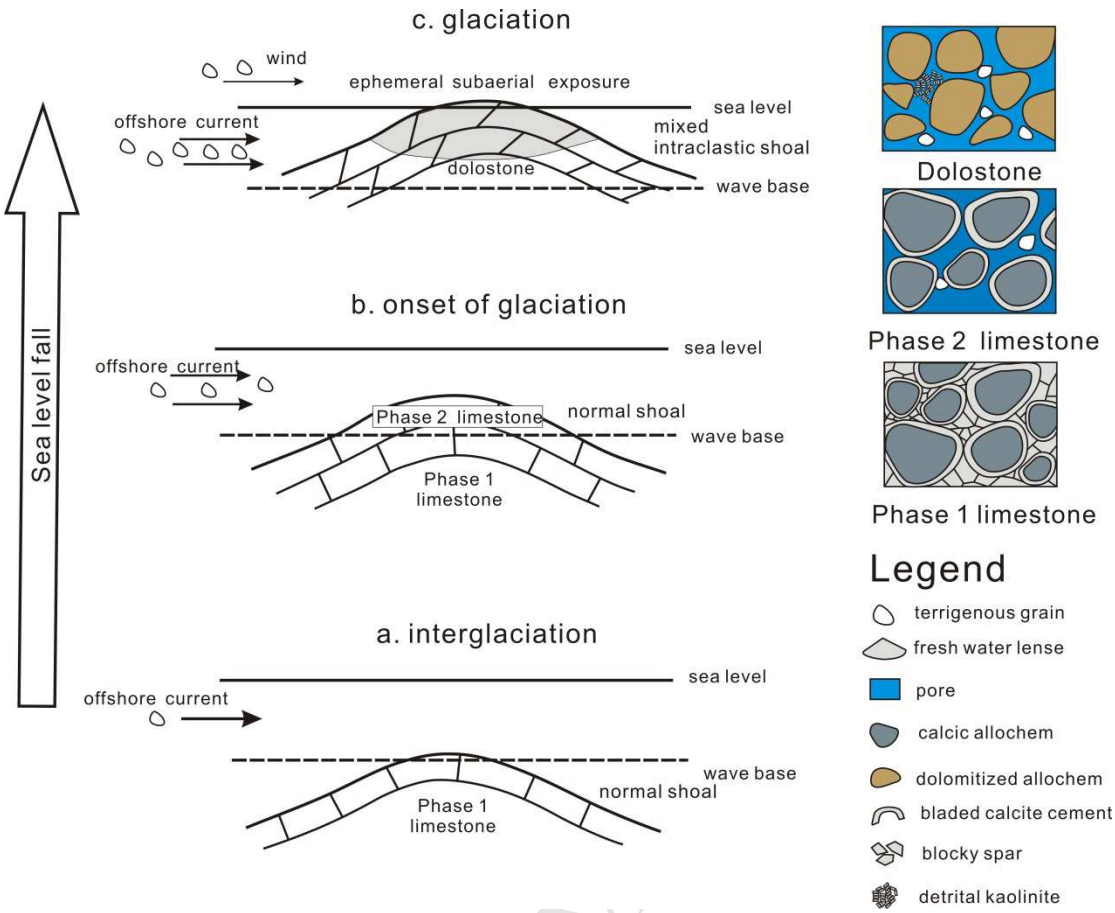

Fig.14 The depositional and diagenetic model of the Xiaohaizi Formation during the cycle of interglaciation and glaciation. The mixed siliciclastic-carbonate sedimentation and subaerial exposure controls the formation of porous dolostones, as response to the sea level fall with proceeding of glaciation. Dolostones with weak cementation have abundant pores to be the best reservoir rocks.

(1) The mixed sedimentation on the carbonate shoals could influence the physical property of reservoirs.

(2) Reservoir quality was controlled by mixed sedimentation and dolomitization associated with glacio-eustatic fluctuation.

(3) Evidences for the emergence of dolostones include vadose silt. palaeosol, karst breccia, detrital kaolinite, darkening of dolostones, and positive $\delta^{18}O\text{-}_{carbonate}$.